2-1-2019

First principles insights on CO adsorption on metal surfaces

Kareem Gameel

School of Sciences and Engineering

Department of Physics

First Principles Insights on CO Adsorption on Metal Surfaces

A Thesis in
Physics

By

Kareem Gameel (B.Sc. in Energy and Renewable Energy Engineering)

Submitted in Partial Fulfillment of the Requirements for the Degree of
Master of Science in Physics

September 2018

The thesis of Kareem Mahmoud Gameel* by the following:

Nageh K. Allam
Associate Professor
Physics Department
Thesis Advisor
Chair of Committee

Adel Awad
Professor
Physics Department
Internal Examiner

Mohamed Elshakre
Professor
Chemistry Department
Cairo University
Internal Examiner

Mohamed Alfiky
Assistant Professor
Physics Department
Moderator

*Signatures are on file in the Graduate School

ABSTRACT

Density functional theory (DFT) has been regularly exploited for meticulous studying of complex surface interactions at a molecular orbital scale. However, DFT calculations usually yield inaccurate thermodynamics results that contradict experimental findings. A clear example is the *CO adsorption puzzle* caused by the wrong estimation of adsorption sites, especially for the (111) transition metal surfaces. The puzzle is still not fully resolved and a complete adsorption picture is yet to be reported.

Herein, we demonstrate the reliability of DFT calculations for the study of local bond properties, despite the wrong energetics predictions. We also highlight the importance of considering a comprehensive analysis of all the possible adsorption sites over distinctive surface facets. Each surface facet, with its unique arrangement of atoms, results in a varying adsorbate behavior, although the same adsorption site is studied. Investigating these variations gives insights about the influence of surface atomic arrangement on the orbitals' interactions. Within the investigation, it is found that the varying density of orbitals, with the matching symmetry for interaction at different adsorption sites, affects the magnitude of orbital interaction, and thus, acts as an additional factor for determining the site preference. Based on the frontier (5σ and $2\pi^*$) orbital energy description, calculated using RPBE functional, new perceptions to the understanding of the *adsorption puzzle* have been exposed. In addition, we emphasize the significance of considering a holistic analysis of adsorbate orbitals, not only limited to the main CO frontier orbitals. This approach leads to a better understanding of the surface bonding and CO final structure. This investigation can help in providing guidelines for innovating design principles for materials, based on the required adsorbate behavior and charge transport phenomena, to be used for catalysis and sensors applications.

TABLE OF CONTENTS

LIST OF FIGURES

LIST OF TABLES

ACKNOWLEDGEMENTS

This work would have never been presented before the reader without the support and funding I was given by the American University in Cairo, which provided the educational and research atmospheres required for excelling in the field of physics. I am grateful for the great professors who assisted in building the necessary theoretical knowledge that constitutes the foundation of a genuine scientist. On the research side, I am sincerely grateful for working with a top-quality professor like Prof. *Nageh Allam*, as my thesis advisor. From day one, he provided guidance with sincere care, while building strong work ethics and research skills. Dr. *Nageh's* availability never ceased to stop 24 hours and throughout the whole week including weekends and holidays; indeed, he is a one pronounced example for dedication and devotion for science and research, and for building a powerful research generation of successful leaders who can survive and even excel in their fields at the most harsh and stressful environments. I would also like to acknowledge the generous support I received from Prof. *Mohammad Shakre,* who provided valuable and meticulous comments on my thesis work within a very short period of time.

I would also like to acknowledge the support I got from my team-mates at the Energy Materials Laboratory (EML). I am particularly grateful for having the chance to collaborate with the theoretical sub-group of the EML in the learning and publishing processes. Moreover, I would like to express my sincere gratitude to my cheering wife (*Nadine*) for her loving support. Finally, I would like to express my gratefulness for my family, particularly my father, who implanted the love of science in me and to whom I appreciatively dedicate this work.

Chapter 1

Introduction

1.1 Scope of the Thesis

This thesis is aimed at addressing the carbon monoxide (CO) adsorption mechanisms from a fundamental level of molecular orbital interactions and charge transfer. This study is executed from an entirely "*theoretical*" perspective, where theoretical methods are utilized for system modeling and electronic structure calculations. The results are then investigated to provide theoretical physical chemistry insights on the adsorption picture of molecules on surfaces. Building a complete molecular orbital picture of adsorption mechanism is, indeed, insightful for enhancing the understanding of surface interaction that can he applied in several applications, most importantly; catalysis. Specifically, the work in this thesis focuses on transition metals as the substrate surfaces for adsorption investigations of CO molecules.

Solids are widely used as catalysts. At their surfaces and interfaces, most of the important chemical reactions in nature and technology take place. The solid surface provides a fertile platform where multiple step reactions can take place[1–3]. Many important phenomena, such as electrode processes, corrosion, heterogenous catalysis, crystallization and dissolution occur at solid interfaces. The acceleration rate of chemical reactions occurring at the solid surface is strongly dependent on the type of surface. That is why industry heavily relies on solid catalysts to produce most of its important chemical

products. In order to manipulate the surface chemical product and its rate of production, the type of solid and the of surface must be meticulously studied. The field of surface chemistry, which is the science of surface and interface interactions, is thus a significant field and is hugely exploited in industry.

In order to understand surface reactions, we need to draw a complete picture of the fundamental atomic and molecular interactions at the surfaces[4]. Understanding the chemical interactions from molecular orbital principles can help in determining the final properties and reactivity of the adsorbed entities. Complex electronic structure investigations, thus, require tools with high accuracy that can grasp the detailed electronic structure perturbations and charge transfers[5,6]. In order to make a profound theoretical – molecular orbital based – analysis, investigation of ground state energies and the electronic structures of the isolated CO molecule, the bare metal surface, and the CO-metal complex is required[7]. Also, the contribution of individual atomic orbitals of both the substrate and adsorbate atoms must be explicitly studied in order to develop a consistent electronic structure model of CO adsorption[8]. This explicit electronic structure and atomic population analysis was believed to be experimentally impossible until the appearance of x-ray emission spectroscopy (XES), which was utilized by scientists during the last two decades, enabling them to extend the conceptual model of the surface chemical bond[5,6]. However, a lot of complications and inabilities, while studying particular atomic and molecular orbitals, were evolving that still make it difficult to reach the ultimate goal of a complete understanding of CO adsorption on metal surfaces. Therefore, a more insightful technique that can provide a better detailed investigation of the electronic structure, accurately, is still needed.

What directly comes into mind is the use of the well-known computational method, the density functional theory (DFT). This technique provides additional tools that can be utilized for both detailed quantitative and qualitative analysis of the CO adsorption on different surface facets and adsorption sites. This makes DFT applicable to offer a wider insight of the underlying physical chemistry of the adsorption mechanisms from a molecular orbital level. Although DFT can provide the detailed molecular orbital calculations required, accuracy related problems are noticeable, making the dependence on this technique for bonding analysis purposes rather questionable[9]. The well-known inherent problem of DFT is that it fails to describe the correct position of energy levels for the studied system. This inaccuracy of DFT calculations can result in wrong energetics calculations, and consequently, wrong site preference of CO adsorption. This problem is manifested in the CO adsorption on the (111) transition metal surface facets, often referred to as the *CO adsorption puzzle*[10–12].

In the present thesis, we demonstrate how we can utilize DFT to carry reliable and meticulous investigations of electronic and structural properties of adsorbates when interacting with transition metal surfaces. Also, we demonstrate how we can exploit the inaccuracies in the predicted electronic structures to decipher the DFT adsorption puzzle and to gain a deeper understanding of the molecular interactions at surfaces.

1.2 Surface Interactions

A variety of materials can make up the surface, including pure metals such as Cu and Pt, ionic such as TiO_2, covalent bonded solids such as Si and Ge, or semimetal such as graphene. Not only does the catalyzed chemical product depend on the nature of the surface, but also it depends on the amplitude of overlap between the electron clouds of the surface and adsorbate species. If the amplitude of electron cloud overlap is above a certain threshold, then the type of interaction is called "*chemisorption*", and if the overlap of electron clouds is negligible, then the type of adsorption is then called "*physisorption*"[13]. Chemisorption and physisorption are thus the main two categories of adsorption on surface. Since physisorption is a weak Van der Waals interaction that induces negligible structural changes on the adsorbed species, in most of the catalysis applications the focus is usually on chemisorption processes, as the higher degree of interactions induces both structural and electronic changes on both the surface and adsorbate species essential for producing the required chemical product.

In chemisorption, where the surface-chemical bond is strong, the investigation of perturbations occurring to the geometric and electronic structures of the metal and adsorbate species is the focus of this thesis. Despite the fact that the surface atoms of the substrate are bound together by highly delocalized valence electrons that form the metallic bonding, the adsorbate molecule can form local bonds with the surface atoms, similar to those formed in organometallics.

When a molecule is adsorbed on the surface, both structural and electronic perturbations occur for both the substrate and adsorbate molecules[1]. During the adsorption

process, the adsorbing molecule may dissociate and violent things can happen to the surface too; phonons and electron-hole pairs can be excited, charge can be exchanged between the surface and adsorbate molecules, and new electronic states can be formed due to the surface chemical bond. Therefore, a detailed understanding of the electronic structure of atoms and molecules is essential for a meticulous description of the surface chemical bonding. That is why, for a deep and detailed understanding of the surface chemical bonding, essential tools for describing the electronic structure of atoms and molecules from a molecular orbital level are essential.

1.2.1 Theoretical Studies for Surface Interactions

The study of molecular surface science has made huge progress in the past 40 years. This development can be attributed to the revolution of experimental techniques that resulted in a significantly better understanding of the fundamental knowledge of simple model systems. In addition, the last 20 years have witnessed a similarly rapid development in the theoretical quantum mechanical based methods, such as density functional theory (DFT)[14]. The theoretical methods provided an extra dimension to obtain wealthy investigation and analysis of data, that resulted in a deeper and more meticulous understanding of the surface chemical phenomena. The purpose of the present investigation is to show how we can utilize theoretical methods, such as DFT, along with the existing experimental techniques for a deeper understanding of surface chemical bonding and how it can be applied in a range of applications, such as electrochemistry, environmental science, semiconductor processing, and heterogenous catalysis.

The knowledge of the geometrical surface and adsorbate structures is the elementary step towards a correct description of the electronic structure and the associated chemical properties of surface-adsorbate complex. These structures are obtained using experimental techniques or by using *ab initio* methods that obtains the lowest energy configuration by varying the position of atoms while calculating the surface energies. Once the ground state configuration is optimized, the obtained structure then forms the basis of the calculation of electronic and chemical properties. Despite the simplicity and effectiveness of the theoretical model of the ground state configuration, experimental tests for these structures is essential to validate the integrity of the calculations[1].

The importance of the surface structure is manifested on the adsorption site, or "*active site*", upon which adsorption occurs. It is found that the adsorption process is significantly modified according to the active-site. In heterogenous catalysis, key steps of surface chemical interactions occur at specific active sites. Thus, the understanding of the effect of the geometry of the active site is essential for the development of catalytic materials[1].

1.3 Electronic Structure Investigations

The main approach to study local bonding properties is through the investigations of the electronic structure of the specific atoms and the specific interacting orbitals. In this chapter, the pros and cons of experimental and theoretical techniques used for electronic structure analyses are presented and compared in terms of accuracy, convenience, and reliability. XES techniques has been utilized by Nilsson and Petterson[15–17] to test for the

assumptions for the proposed adsorption models, such as the Blyholder model[18], which assumes a simple two-step charge σ donation and a 2π* back-donation interaction. The nature of the new electronic states formed upon adsorption were also tested and the perturbations to the remaining orbitals were also monitored. The XES analyses conclusions reported that the simplistic Blyholder model is actually neither correct nor complete; incorrect in the sense that the σ donation is a rather repulsive interaction and the description of the backdonation should involve all the π orbitals and not only the 2π* orbital. Based on the breakage of the Blyholder model assumption, new – more complete – picture of the surface chemical bond for CO on transition metal surfaces.

1.3.1 Experimental Techniques

X-ray spectroscopy (XAS), X-ray emission spectroscopy (XES)[1,7,19–22], and laser-induced desorption[23] yield experiments are the main techniques utilized to investigate electronic structure for the analysis of the bonding processes[24]. Before the introduction of photoelectron spectroscopy (XPS) in the early 20th century, the XES tool was the method of choice for studying electronic structure in matter[25].

XAS is used to investigate the unoccupied density of states, where a core electron gets excited to an empty level. XES, on the other hand, is used to investigate the occupied density of states, where an electron in a higher occupied state relaxes to fill the position

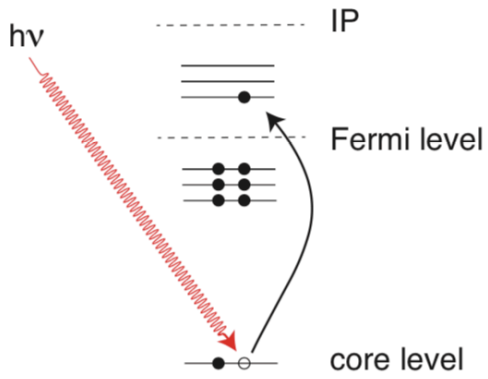

Figure 2 XAS process occurring when a core electron is excited to a higher unoccupied level and the formation of a core-hole at the original position[21]

(core-hole) of a precedingly excited core electron by XAS. *Figure 2*. and *Figure 1* show the three chronological steps of core electron excitation by XAS to higher level above the fermi level, then the formation of a core-hole at the original position of the excited core-electron, which is followed by the relaxation of an electron at higher occupied state by XES to take the core-hole position, resulting in an emitted photon.

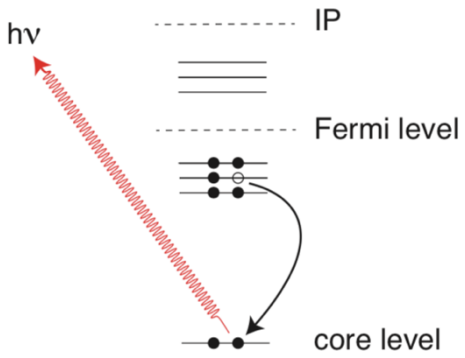

1.3.2 Theoretical Techniques

Despite the great advancements in experimental techniques, these techniques are not sufficient to grasp the complete electronic structure picture required. Due to dipole selection rules, only specific angular momentum contributions can be observed[15]. Therefore, the behavior of certain atomic orbitals cannot be monitored and investigated. In addition, mixing of different atomic orbitals usually take place, which makes viewing the complete electronic structure picture very complex; subtraction of spectra is then required[17]. Therefore, XES applied to monolayers and surfaces can be experimentally very demanding. Furthermore, adsorption of molecules can only be studied on the experimentally preferred adsorption sites, and the freedom of further "imaginal" investigations on thermodynamically un-preferred sites cannot be achieved.

On the other hand, theoretical methods can fill all the gaps in experimental techniques. Using theory, we can generate pure, complete, and symmetry-resolved spectra, which offers a wider insight for the underlying physical chemistry of the adsorption mechanisms from a molecular orbital level[17]. The spectra of individual orbitals – the density of states (DOS) data - can then be summed up and compared to experimental data. Additionally, we can theoretically study adsorption on the thermodynamically non-preferred adsorption sites, which can answer the question of why molecules tend to prefer adsorption on specific adsorption sites over the others. Computational chemistry tools have developed into a powerful tool for meticulous atom by atom investigations. A common practice that has been employed is to utilize both experimental and computational

techniques for a more profound investigation. A calibration of theoretical methods (DFT) against experiment and the details of the remaining orbitals' contributions can be obtained from various orbital symmetries.

Although DFT can provide the detailed molecular orbital calculations required, but accuracy related problems are noticeable, making the dependence on this technique for bonding analysis purposes rather questionable[4,26]. There are two challenges that face the theoretical description of the surface-adsorbate complex: first is the correct description of electronic bandgap between the HOMO-LUMO orbitals' positions of the adsorbed molecule, and second is the correct description of the electronic structure of the transition metals. Because of their open *d*-shells and accompanying spin-coupling, near-degeneracy and dynamical correlation problems, predictions of the electronic structure of transition metals is rather difficult[17]. Consequently, most semilocal exchange-correlation (xc) density functionals underestimate surface energies and predict them to be more stable than they actually are[26]. Correct description of adsorbate-substrate interactions was only achieved using more accurate Hybrid functional calculations, only for Cu with its closed *d*-shell configurations and failed with other open *d*-shell transition metals[27]. Therefore, theoretical adsorption investigations on Cu can provide a good reliability for comparisons with more reactive metals, such as Ni and Pt.

1.4 Carbon Monoxide as an Adsorbate

The mostly studied prototypical model in Surface Chemistry field is the adsorption of the CO molecule. In chemistry, we always aim for the simplest models for scientific investigations. In addition, the complexity of adsorption investigations grows steeply with the number of atoms within the adsorbate molecule[3]. However, this simple model must be easily and clearly tested experimentally. For example, taking H as the simplest model for adsorption can be valid, however, H atoms are exceptionally weak scatterers of electrons and have no electronic core level[17]. So, it is extremely difficult to utilize spectroscopic techniques to investigate the adsorption of H atoms on surface. On the other hand, the most studied molecular adsorbate structure is the CO. From a structural perspective, the CO molecule is a rather simple species with two distinct atoms; carbon and oxygen. Particularly, the CO adsorption on transition metal surfaces is important in the heterogenous catalysis context.

Other than the theoretical convenience of CO adsorption model for the theoretical description of adsorption, the adsorption of CO is also a vital case study in surface science. This is because CO adsorption is considered an essential part in CO oxidation catalysis applications. One of these applications is the CO_2 electro-reduction (ER) into hydrocarbon (HC) fuel[28,29]. This reaction has a considerably low overall efficiency, and an optimum catalyst that can improve the efficiency to the extent that is high enough to be commercialized is yet to be discovered. CO_2 ER process to HC involves multiple reaction steps, and the protonation of CO*, that occurs after the formation of CO on the electrode

surface, is considered the rate limiting step. In addition, catalysis using transition metals has been widely utilized to lower the emissions of CO in automobile exhausts.

1.4.1 CO Molecular Orbital Picture

As depicted in *Figure 3*, the CO molecule is formed by the triple bonding of one carbon atom with one oxygen atom. Eight molecular orbitals are formed by the interaction of the occupied s and p orbitals of oxygen and carbon. The internal C-O triple bond is held by the fully occupied 1π and 3σ orbitals. One of internal triple bond is due to an oxygen dative (coordinate) covalent bonding. That dative bonding causes the formation of a dipole moment towards the carbon end, despite the higher electronegativity of oxygen. The highest occupied molecular orbital (HOMO) is the 5σ, while the lowest unoccupied

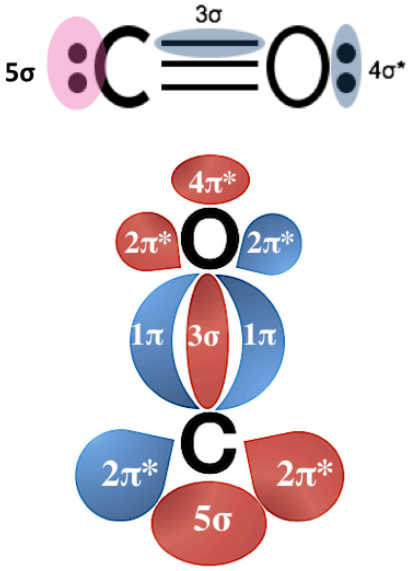

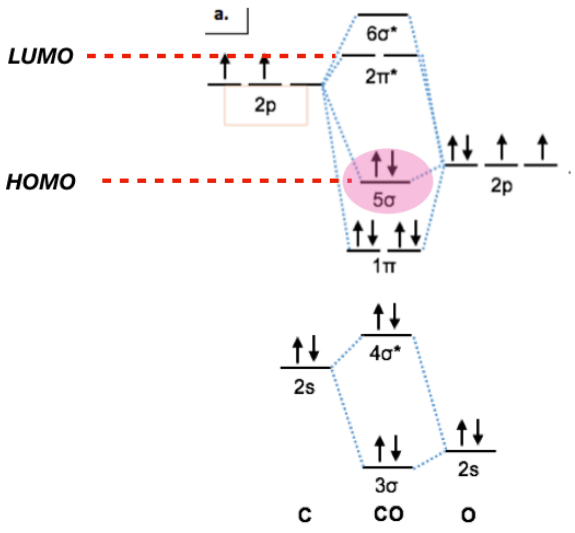

molecular orbitals are the $2\pi^*$ orbitals. The HOMO and LUMO orbitals play an essential role in the interaction with the atoms of solid surfaces.

1.5 CO Adsorption Model

The single most successful model that provides a valid description of the adsorption mechanism is the Blyholder model of CO adsorption[18]. The Blyholder model, has been further refined by Nilsson and Petterson to make the combined Blyholder-Nilsson-Petterson (BNP) model[15].

1.5.1 The Blyholder Model

As depicted in *Figure 4*, the Blyholder model describes the adsorption process through a two-step reaction; beginning with a donation of electrons from the 5σ orbital of

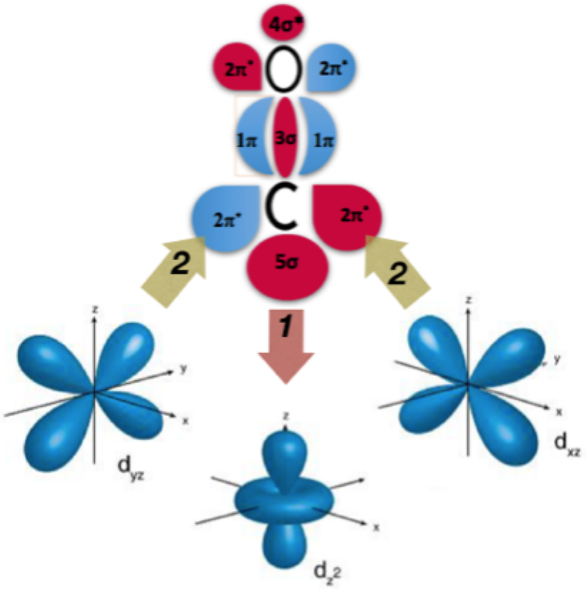

the CO to the metal followed by a back-donation of charge from the metal to the $2\pi^*$. In the adsorption model, synergism between σ and π is achieved, where the internal C-O bond is weakened due to the increased population of $2\pi^*$ due to charge back-donation from the metal atoms. This claim can be validated by observing the degree of internal bond weakening as the coordination number increases. For symmetry arguments, the vertically directed 5σ interaction is particularly strong for atop adsorption. As the coordination number increases, the $2\pi^*$ orbitals have more significant spatial proximity to the metal *d*-orbitals, where the degree of back-donation increases with the increase of the number of bonding metal atoms, as shown in *Figure 5*. This increase of the number of bonding atoms results in an increased population of the $2\pi^*$ orbitals, which results in the weakening of the internal C-O bond, due to its antibonding character.

1.5.2 The Nillson-Petterson Model

The simplistic Blyholder model has been refined by Nilsson and Petersson[15], who succeeded in extending the conceptual model of the surface chemical bond. In their studies, they showed that the adsorbate substrate complex is destabilized by σ- interactions and stabilized by π-interactions. They also proved that the π-bonding is manifested through the creation of a d_π band formed by the hybridization of the 1π and 2π orbitals with the metal *d*-states. The σ-bonding, on the other hand, is formed due to the formation of a d_σ band formed by the hybridization of the 4σ and 5σ orbitals with the metal *d* states. The balance between σ- repulsion π-attractions is what governs the equilibrium properties of the CO adsorbed on metals and their adsorption energies.

Therefore, both the Blyholder and Nilsson-Petersson models concentrate mainly on the interaction of frontier orbitals with the metal *d*-states, while overlooking the interaction with the broad metal *sp* states. Stroppa *et al*[27] showed that the $2\pi^*$ cannot interact with the *s* or p_z orbitals for top-site adsorption, however for high-coordination sites, $2\pi^*$-sp_z are stronger, since antisymmetric combinations are available at these sites.

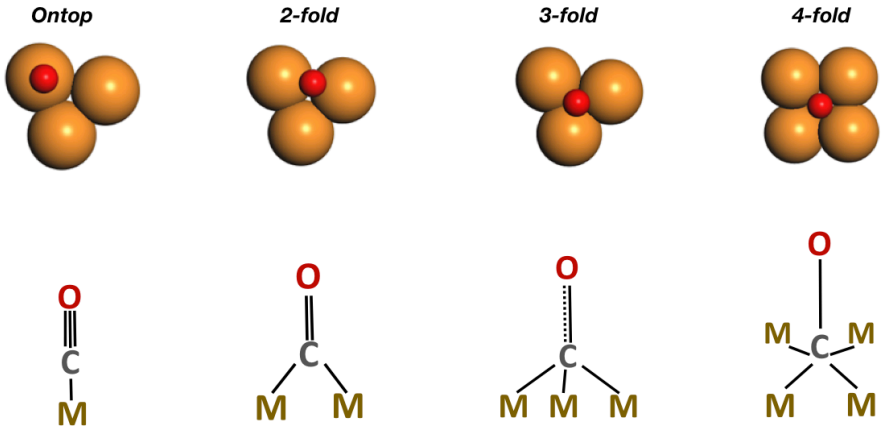

References

1. Nilsson, A. *et al.* Probing chemical bonding in adsorbates using X-ray emission spectroscopy. *J. Electron Spectros. Relat. Phenomena* (2000). doi:10.1016/S0368-2048(00)00155-9
2. Sholl, D. S. & Steckel, J. A. *Chapter 03: Nuts and Bolts of DFT Calculations*. *Density Functional Theory: A Practical Introduction* (2009). doi:10.1002/9780470447710.ch3
3. Norsko, J. K. Chemisorption on metal surfaces. *Reports on Progress in Physics* **53,** 1253–1295 (1990).
4. Stroppa, A. & Kresse, G. The shortcomings of semi-local and hybrid functionals: What we can learn from surface science studies. *New J. Phys.* (2008). doi:10.1088/1367-2630/10/6/063020
5. Föhlisch, A. *et al.* Ground-state interpretation of x-ray emission spectroscopy on adsorbates: CO adsorbed on Cu(100). *Phys. Rev. B - Condens. Matter Mater. Phys.* **61,** 16229–16240 (2000).
6. Föhlisch, A. *et al.* How carbon monoxide adsorbs in different sites. *Phys. Rev. Lett.* **85,** 3309–3312 (2000).
7. Wiell, T. *et al.* Local probing of adsorbate electronic structure using soft X-ray emission; atomic nitrogen on Ni(100) and Cu(100). *Surface Science* (1994). doi:10.1016/0039-6028(94)91326-9
8. Stroppa, a, Termentzidis, K., Paier, J., Kresse, G. & Hafner, J. CO adsorption on metal surfaces: a hybrid functional study with plane wave basis set. *Phys. Rev. B*

76, 32 (2007).

9. Tolba, S. A., Gameel, K. M., Ali, B. A., Almossalami, H. A. & Allam, N. K. The DFT+U: Approaches, Accuracy, and Applications. in *Density Functional Calculations - Recent Progresses of Theory and Application* (ed. Yang, G.) (IntechOpen, 2018). doi:10.5772/intechopen.72020
10. Feibelman, P. J. *et al.* The CO/Pt (111) Puzzle. *J. Phys. Chem. B* (2001). doi:10.1021/jp002302t
11. Hu, Q. M., Reuter, K. & Scheffler, M. Towards an exact treatment of exchange and correlation in materials: Application to the 'cO adsorption puzzle' and other systems. *Phys. Rev. Lett.* (2007). doi:10.1103/PhysRevLett.98.176103
12. Lazić, P. *et al.* Density functional theory with nonlocal correlation: A key to the solution of the CO adsorption puzzle. *Phys. Rev. B - Condens. Matter Mater. Phys.* **81,** (2010).
13. Groß, A. *Theoretical surface science: A microscopic perspective*. *Theoretical Surface Science: A Microscopic Perspective* (2009). doi:10.1007/978-3-540-68969-0
14. Geerlings, P., De Proft, F. & Langenaeker, W. Conceptual Density Functional Theory. *Chem. Rev.* (2003). doi:10.1021/cr990029p
15. Föhlisch, A. *et al.* The bonding of CO to metal surfaces. *J. Chem. Phys.* **112,** 1946–1958 (2000).
16. Föhlisch, a. *et al.* Ground-state interpretation of x-ray emission spectroscopy on adsorbates: CO adsorbed on Cu(100). *Phys. Rev. B* (2000). doi:10.1103/PhysRevB.61.16229

17. Anders Nilsson, Lars G.M. Pettersson & Jens K. Nørskov. *Chemical Bonding at Surfaces and Interfaces*. (2008).

18. Blyholder, G. Molecular Orbital View of Chemisorbed Carbon Monoxide. *J. Phys. Chem.* (1964). doi:10.1021/j100792a006

19. Wiell, T. & Klepeis, J. Local aspects of the adsorbate-substrate chemical bond in N/Cu(100) and O/Cu(100). *Phys. Rev. B - Condens. Matter Mater. Phys.* (1998). doi:10.1103/PhysRevB.58.1655

20. Bennich, P. *et al.* Nature of the surface chemical bond in N-2 On Ni(100) studied by x-ray-emission spectroscopy and ab initio calculations. *Phys. Rev. B* (1998). doi:10.1103/PhysRevB.57.9274

21. Nilsson, A. *et al.* An atom-specific look at the surface chemical bond. *Phys. Rev. Lett.* (1997). doi:10.1103/PhysRevLett.78.2847

22. Tillborg, H. *et al.* Electronic structure of atomic oxygen adsorbed on Ni(100) and Cu(100) studied by soft x-ray emission and photoelectron spectoscopies. *Phys. Rev. B* (1993). doi:10.1103/PhysRevB.47.16464

23. Gladh, J., Hansson, T. & Öström, H. Electron- and phonon-coupling in femtosecond laser-induced desorption of CO from Ru(0001). *Surf. Sci.* (2013). doi:10.1016/j.susc.2013.05.002

24. Gladh, J. Bonding and Desorption Mechanisms of CO on Metal Surfaces. (Stockholm University, 2012).

25. Nilsson, A. & Pettersson, L. G. M. Chemical bonding on surfaces probed by X-ray emission spectroscopy and density functional theory. *Surface Science Reports* (2004). doi:10.1016/j.surfrep.2004.06.002

26. Schimka, L. *et al.* Accurate surface and adsorption energies from many-body perturbation theory. *Nat. Mater.* **9,** 741–744 (2010).

27. Stroppa, a, Termentzidis, K., Paier, J., Kresse, G. & Hafner, J. CO adsorption on metal surfaces: a hybrid functional study with plane wave basis set. *Phys. Rev. B* **76,** 32 (2007).

28. Akhade, S. a *et al.* Poisoning effect of adsorbed CO during CO2 electroreduction on late transition metals. *Phys. Chem. Chem. Phys.* (2014). doi:10.1039/c4cp03340j

29. Kortlever, R., Shen, J., Schouten, K. J. P., Calle-Vallejo, F. & Koper, M. T. M. Catalysts and Reaction Pathways for the Electrochemical Reduction of Carbon Dioxide. *J. Phys. Chem. Lett.* (2015). doi:10.1021/acs.jpclett.5b01559

Chapter 2

Background*

2.1 Theoretical Methods

The total energy of the system is the fundamental quantity that can lead us to grasp all of the static properties of that system and can further lead us to predict the changes occurring on a time scale. The accuracy of the theoretical predictions for a system, therefore, basically relies on the accuracy of the energy description. For a system containing a number of particles, the energy of the system, is solely described as the summation of the kinetic energy of the individual particles and the potential energy experienced by each particle[1–3]. If an interaction between particles of the system exist, the potential energy term becomes more complicated to describe. The potential energy term can become even more complicated when dealing with quantum mechanical particles, like electrons. In this case, the kinetic and potential energy terms of these massless particles are described by quantum mechanical wave-equations that govern the system dynamics of systems.

Quantum mechanics is considered the most profound scientific advancement of the 20th century[4]; experimental observations have confirmed that this theory of matter profoundly and accurately describes the universe in which we live in. For a non-relativistic system, the ground-state energy can be obtained by simply solving the Schrodinger equation. For a system of one or two particles, the Schrodinger equation can be solved

* Parts of this chapter were published in the following book chapter: Kareem M. Gameel*, Sarah A. Tolba*, Basant A. Ali, Hossam A. Almossalami, Nageh K. Allam, "*The DFT+U: Approaches, Accuracy, and Applications",* Book Chapter in the *"DFT Calculations: Recent Progresses of Theory and Application*" Intech Book, Edited by Gang Yang, May 2018.

exactly, and the ground state energy and the properties of the system can be theoretically correctly predicted. However, for a system larger than that, exact solution for the energy of the system becomes unattainably complex and approximations have to be employed.

2.1.1 The Hamiltonian

The Hamiltonian is the central quantity of any theoretical treatment; it contains all the information about the system under consideration with all the details of fundamental interactions present in that system. When the Hamiltonian is defined, all the chemical and physical properties of the system can be derived. Since we are dealing with systems that are composed of atoms and electrons for surface science, this microscopic scale is governed by quantum mechanical laws of physics, and therefore, must be described by solving the Schrodinger equation. Therefore, for surface science theoretical investigations, we need to define the appropriate Schrodinger equation and Hamiltonian with their specific forms for describing surfaces[4,5]. The first step towards making the solution of the Schrodinger equation more tractable is the decoupling of the electronic and nuclear motion using the Born-Oppenheimer approximation.

2.1.2 The Schrodinger Equation

The most critical part of the Schrodinger equation for solid state physics or chemistry computations is the electrostatic interaction term. In the case of considering only valence electrons interactions, relativistic effects are usually neglected. As a preliminary

step for simple description of the Hamiltonian, we neglect any magnetic (spin) effect for both valence and core electrons. With nuclei and valence electrons being set, the system can be described with a non-relativistic time independent Schrodinger equation with a Hamiltonian with a well-defined form of five terms, two of them are kinetic energy terms and the other three are potential energy terms:

$$H = T_n + T_e + V_{n-n} + V_{n-e} + V_{e-e} \qquad (2.1)$$

Each of the four terms is described by the following formulae, while neglecting the spin property for the sake of simplicity and clarity:

$$T_n = \sum_{I=1}^{L} \frac{P_I^2}{2M_I}$$

$$T_e = \sum_{i=1}^{N} \frac{p_i^2}{2m} \qquad (2.2)$$

$$V_{n-n} = \frac{1}{2} \sum_{I \neq J}^{N} \frac{Z_I Z_J e^2}{|R_I - R_J|}$$

$$V_{n-e} = -\sum_{i,I} \frac{Z_I e^2}{|r_i - R_I|}$$

$$V_{e-e} = \frac{1}{2} \sum_{i \neq j} \frac{e^2}{|r_i - r_j|} \qquad (2.3)$$

The atoms are numbered in capital letters indices, i.e. Z_I stands for the charge of the Ith electron. For the $V_{n\text{-}e}$ and $V_{e\text{-}e}$ expressions, the factor of ½ is introduced to cancel out the double counting of interaction between the same pair of particles. By defining those four terms, we can, in principle, solve the many-body Schrodinger equation and get the energy of the system using the Hamiltonian:

(2.4)

$$H\Phi(R,r) = E\Phi(R,r) \qquad (2.7)$$

However, for the above expressions for electronic kinetic and potential energies, all physical information is included except for the symmetry of the wavefunctions. Since electrons are fermions, quantum statistics should be included, such as the Pauli principle. This proper consideration of the quantum statistics leads to the inclusion of an important energy term known as the *exchange-correlation* term that significantly affects the so-called *effective Hamiltonian.* In addition, usually relativistic effects are neglected, and only in the cases of heavier elements with very localized wavefunctions considered for core electrons, relativistic effects become more significant and needs to be considered because of the high kinetic energies of the core electrons due to localization. These effective terms are derived from the energy difference (energy cost) between the energies of the system with and without the inclusion of quantum statistics.

Solving the many-body Schrödinger equation is unfortunately impossible in its closed form and a hierarchy of approximations that can make the solution possible within an acceptable accuracy must be employed. The primary step in this hierarchy is the so called Born-Oppenheimer approximation[5].

2.1.3 Born-Oppenheimer Approximation

Generally, atoms have a mass that is 10^4 to 10^5 times larger than the mass of an electron, except for hydrogen and helium, which makes the kinetic energy of electrons 10^2 to 10^3 times larger than the nuclei[5]. Therefore, we can suppose that the electron follows the motion of the nuclei almost immediately and that the electrons are in their ground state for

any configuration of the nuclei. The electronic state then defines the potential in which electrons move. Therefore, the separation of time scales of processes involving electrons and atoms is the key idea behind the Born-Oppenheimer or adiabatic approximation.

Now, the new Hamiltonian will be short of one kinetic energy term, which is that of the nuclei. Implying that nuclei are pictured static and that only electrons are moving. So, the new Hamiltonian, with fixed nuclear coordinates $\{R\}$ is now called the *electronic* Hamiltonian H_e and will look like this:

$$H_e(\{R\})\psi(r,\{R\}) = E_e(\{R\})\psi(r,\{R\}) \qquad (2.8)$$

In the above equation, the $E_e(\{R\})$ is the electronic potential in which nuclei are moving, i.e. the $E_e(\{R\})$ is the Born-Oppenheimer energy surface.

To probe nuclear motion, the so called "atomic" Schrodinger equation must be solved, where quantum effects in the atomic motion are neglected and classical equations of motion are solved for the nuclear motion. The validity of the Born-Oppenheimer approximation is hard to prove since it neglects electronic transitions due to nuclear motion, which makes it difficult to describe process involving electronic transitions. Nonetheless, the Born-Oppenheimer approximation is successful for the theoretical prediction of surface processes[5].

2.1.4 Structure of the Hamiltonian

The Born-Oppenheimer approximation implies that nuclear positions are fixed and that we can now solve for the so-called electronic Hamiltonian. The electrons in the system are now moving in an external electrostatic potential determined by the fixed atomic

positions. In addition, these fixed atomic positions determine the symmetry properties of the Hamiltonian.

Systems studied in surface science are composed of two entities that are described by two distinctive computational methods; the molecules are treated with quantum chemistry methods, while surfaces are handled using solid state methods. These different methods exist because of the different degrees of freedom possessed by each entity; the atom or molecule interacting with the surface has an infinite number of degrees of freedom, while the solid-state surface has only few degrees of freedom. Handling both subsystems in one model, thus, represents a real challenge for any theoretical treatment. One initial step that can drastically simplify the system model and as well reduce the computational cost is the consideration of symmetry.

The determination of the total energy of a system is the fundamental preliminary step for the theoretical treatment of any property of that system. The electronic structure is the basic property that is used for determining the total energy. The electronic structure methods are divided into two main categories: wave-function and electron-density based methods that originate from quantum chemistry and solid-state physics, respectively. Since solid surfaces have periodic structure, density functional theory (DFT) methods dominates theoretical surface science.

2.2 Density Functional Theory

Density functional theory (DFT) is the most convenient and computationally least expensive tool utilized by computational materials researcher for electronic structure

calculations for ground state many-body systems[4,6–9]. Instead of the wavefunctions as the fundamental variable for solving the Schrodinger equation, DFT solves the many-body problem using electronic charge density as the fundamental variable[6,7,9,10]. This simple (clever) idea originates from the fact that the electronic structure is unique for each type of material. In the same context, the density of electrons is also unique for each type of material. Therefore, by merely considering the electronic density, we can uniquely and distinctively describe materials properties using density functional theory.

The fundamental goal of quantum mechanics is to solve the Schrodinger equation through solving for the many-body wavefunctions. However, the wavefunction for any set of coordinates cannot be directly observed. In principle, the quantity that can be measured is the probability of N electrons are existing at a particular set of coordinates, $\mathbf{r}_1, \ldots, \mathbf{r}_N$. This probability is equal to $\Psi^*(\mathbf{r}_1, \ldots, \mathbf{r}_N)\Psi(\mathbf{r}_1, \ldots, \mathbf{r}_N)$. It is worth-noting that, in quantum mechanics, electrons are indistinguishable, so we don't care which electron is labelled electron 1 and which is labelled electron 2. Therefore, the quantity of physical interest is basically the probability of N electrons, labelled in any order, have the coordinates $\mathbf{r}_1, \ldots, \mathbf{r}_N$. A typically related quantity of that probability of existing N electrons is the density of electrons at a particular region of space, $n(\boldsymbol{r})$[4]. The density of electrons can be written in terms of the summation of individual electron wavefunctions that are occupied by electrons. Therefore, the term inside the summation is the probability that a distinct electron in an distinct wave function is located at position $\mathbf{r}$, written as follows:

$$n(r) = 2\sum \psi_i^*(r)\psi_i(r) \qquad (2.9)$$

Since electrons are fermions with a spin ½ property, the Pauli exclusion principle states that no two electrons with the same spin can occupy the same orbital (wavefunction), which is the reason why the factor of 2 appears in the equation. This spin effect is a purely quantum mechanical phenomenon that has no classical counterpart. The electron density $n(\boldsymbol{r})$ is a function of only three spatial coordinates that contains a wealth amount of information that is physically observable from the full wavefunction solution to the Schrodinger equation, which is a function of $3N$ coordinates.

2.2.1 From Wavefunctions to Electron Density

The first, and one of the two fundamental mathematical theorems of DFT, theorem proved by Hohenberg and Kohn states the following[4]:

"The ground-state energy from Schrodinger's equation is a unique functional of the electron density."

What this theory implies is that the ground-state electronic structure (wavefunctions), which is unique for each material, can be mapped to the ground-state electron density, which is also unique for each material. To put it in a mathematical form, Hohenberg and Kohn states that the ground state energy E is a function of electron density $n(\boldsymbol{r})$, $E[n(\boldsymbol{r})]$. So, E is a function of another function $n(\boldsymbol{r})$, and the function of a function is called a *"functional"*; and that's where the name of the density functional theory comes from.

Since any material is uniquely described by its unique electronic structure, which is now also mapped to its unique electronic density, all the properties of any material are uniquely determined by its ground-state electronic structure (and electronic density). Therefore, in order to find the properties of a material, instead of solving the Schrodinger equation by finding the wavefunction of 3*N* variables, we can instead solve by finding the electronic density which is a function of 3 spatial coordinates. For example, for a nanocluster consisting of 100 Pd atoms with more than 23,000 dimensions, the problem can be reduced to merely 3 dimensions using the electronic density.

The Hohenberg-Kohn theorem have paved the way to the new idea of the one to one mapping of the ground-state wavefunction to the ground-state electronic density that can be employed to solve the Schrodinger equation. However, the theorem says nothing about what the functional actually is. In order to find the set of wavefunction $n(\boldsymbol{r})$ that corresponds the "true" ground-state electron density, the second Hohenberg-Kohn theorem introduced the variational principle to the energy functional stating the following[4]:

The electron density that minimizes the energy of the overall functional is the true electron density corresponding to the full solution of the Schrodinger equation.

So, the electron density is varied until the energy from the functional is minimized, which corresponds to the ground-state electron density. The ground-state energy of the system is then written in terms of single-electron wavefunctions, $\Psi_i(\mathbf{r})$, where these functions collectively define the electron density, $n(\boldsymbol{r})$. The energy functional is then written as a function of two terms; mathematically *known* and *unknown terms.*

$$E[\{\psi_i\}] = E_{known}[\{\psi_i\}] + E_{XC}[\{\psi_i\}] \qquad (2.10)$$

The *known* term includes four contributions, written in order from left to right in equation (2.11): the electronic kinetic energies, the electron-nuclear Coulomb interactions, the electron-electron interactions, and the nuclear-nuclear interactions, as follows:

$$E_{known}[\{\psi_i\}] = \frac{h^2}{m}\sum_i \int \psi_i^* \nabla^2 \psi_i d^3r + \int V(r)n(r)d^3r$$
$$+ \frac{e^2}{2}\iint \frac{n(r)n(r')}{|r-r'|} d^3r d^3r' + E_{ion} \qquad (2.11)$$

The second term in the complete wavefunction, $E_{XC}[\{\Psi_i\}]$, is the exchange and correlation energy functional, which includes all the quantum mechanical effects that are not included within the known term. Kohn and Sham (KS) showed that the task of finding the right electron density can be expressed by solving a set of equations, in which each equation only involves a single electron:

$$[\frac{h^2}{2m}\nabla^2 + V(r) + V_H(r) + V_{XC}(r)]\psi_i(r) = \varepsilon_i \psi_i(r) \qquad (2.12)$$

This equation only depends on three spatial variables that define the position vector **r**. There are three potential energy terms in the left hand-side bracket. The first one, $V(\mathbf{r})$, is the electron-nuclear interaction energy term, which is the interaction between the electron and the collection of nuclei; this term is part of the *known* energy functional. The second term is, $V_H(\mathbf{r})$, is the Hartree potential term, which is defined by:

$$V_H(r) = e^2 \int \frac{n(r')}{|r - r'|} d^3r \qquad (2.13)$$

This term defines the electronic interaction between a single electron and the mean-field (total density) defined by all electrons in the system. This Hartree term, thus, adds an extra interaction, called the self-interaction, which is due to the inclusion of all the electrons in the mean-field interacting with the electron considered for interaction. Therefore, the electron interacting with itself becomes part of the V_H. The correction of this self-interaction is the inscribed inside the V_{XC} term, which defines the exchange and correlation contributions to the single electron KS equations.

So, in order to solve the KS equation, we need to define the Hartree potential V_H, and to know the V_H, we need to define the true ground-state electron density. This electron density is, however, only found after knowing the single electron wavefunctions, which are only found by solving the KS equations. So, in order to find the solution of this dilemma, we define the following closed loop algorithm, which is defined by the set of the following steps:

1- Make an initial guess of the electron density, $n(\boldsymbol{r})$.
2- Compute the Hartree potential V_H, which is a function of the guessed electron density, $n(\boldsymbol{r})$.
3- Solve the set single-electron KS equation and get a set of single electron wave functions $\Psi_i(\mathbf{r})$

4- Calculate the new electron density, $n(\boldsymbol{r})$, defined by the calculated set of single electron wave functions $\Psi_i(\mathbf{r})$.

5- Plug in the new calculated density $n(\boldsymbol{r})$ and recalculate the V_H, and repeat steps 3 and 4, until the plugged-in $n(\boldsymbol{r})$ is equal to the calculated $n(\boldsymbol{r})$ from the set of single electron wave functions $\Psi_i(\mathbf{r})$ → Self-consistent solution.

However, there are many questions that need to be answered before starting this algorithm:

- How close should the plugged in and calculated electron-densities be, so we can define it as a self-consistent solution?
- How can we make an accurate first guess of the initial electron density?

2.2.2 The Exchange-Correlation Functional

The true existence of the exchange-correlation (xc) functional, proved by Hohenberg and Kohn, is simply not known. The development of a functional that describes the true nature of the xc interaction is currently one of the most active areas of quantum chemistry research. However, there is a single case, where the true xc energy can be known exactly: the uniform electron gas. In this case, the electron density, $n(\boldsymbol{r})$, is constant at all points in space. In real materials science, variations of electronic densities do exist, making the free gas constant electron density an ideal, yet not practical, special case. However, the uniform electron gas provides a way to practically use the KS equations. Practically, at

each special position in the system, we define a known xc-potential from the uniform electron gas at the electron density observed at that position.

$$V_{XC}(r) = V_{XC}^{elec.gas}[n(r)] \qquad (2.14)$$

Basically, this approximation uses only the local density to define the approximate xc functional → Local Density Approximation (LDA). Unfortunately, the LDA functional still do not capture the true nature of the xc functional. Although, we did not yet reach the true mathematical formulation of the xc functional that can work for all systems, there are a number of approximate systems that are widely adopted by theoretical materials researchers, which are found to give fairly accurate (reliable) results. So, the primary skill that the theoretical "users" of these functionals is to know how and when to use the existing xc functionals. One of the most popular functionals that use the information about the local electron density and the local gradient in the electron density is the *generalised gradient apporximation* (GGA). There are many physical system cases, where GGA gives more accurate results than LDA, but this is not always true. There are many ways in which the electron density gradient can be defined, and that's why there are a large number of distinct GGA functionals that produce different results a particular configuration of atoms.

The wave function of an *N*-particle system is an *N*-dimensional function. In order for the wavefunction to correctly provide a correct quantum mechanical description of an *N*-electron system, these wavefunctions must mathematically satisfy the real electronic properties, which should also be true for any approximate form of the wavefunction that we construct.

2.3 DFT Electronic Structure Problem and Corrections

The attainment of a correct description of electronic structure is critical for predicting further electronic-related properties, including intermolecular interactions and formation energies. The chapter begins with an introduction to the formulation of density functional theory (DFT) functionals, while addressing the origin of bandgap problem with correlated materials. Then, the corrective approaches proposed to solve the DFT band-gap problem are reviewed, while comparing them in terms of accuracy and computational cost. The Hubbard model will then offer a simple approach to correctly describe the behavior of highly correlated materials, known as the Mot insulators. Based on Hubbard model, DFT+U scheme is built, which is computationally convenient for accurate calculations of electronic structures. Later in this chapter, the computational and semi empirical methods of optimizing the value of the Coulomb interaction potential (U) are discussed, while evaluating the conditions under which it can be most predictive. The chapter focuses on highlighting the use of U to correct the description of the physical properties, by reviewing the results of case studies presented in literature for various classes of materials.

2.3.1 Accuracy of DFT Electronic Predictions

Although DFT calculations' accuracy is acceptable as long as structural and cohesive properties are concerned, it dramatically fails in the prediction of electronic and other related properties of semiconductors up to a factor of two[11]. However, reaching a

correct description of electronic structure is critical for predicting further electronic-related properties, including intermolecular interactions and formation energies. In order to solve this problem, computationally heavier jobs must be employed, using either larger basis sets or hybrid functionals, which include the solution of the exact Hartree-Fock (HF) equations, in order to reach relatively higher accuracies[4]. Nevertheless, in some cases, even solving exact HF equations can fail in correctly predicting the bandgap for a certain class of semiconductors that possess strong correlations between electrons, such as Mott insulators[12,13]. Consistent research efforts have been employed in order to formulate more accurate functionals, by using corrective approaches or alternatives to the density functionals. The applicability of these alternatives and corrections has large dependence on the type of the system studied, its size and complexity, and the computational cost required. One of the corrective approaches employed to relieve the DFT electronic bandgap problem is the DFT+U correction method, which is the focus of this chapter. Compared to the alternative approaches, such as the hybrid functionals and the post-Hartree-Fock methods, DFT+U correction has proved to be as reliable as the other methods, but with a critical advantage of considerably lower computational cost. By successfully correcting the electronic structure of the studied system using the *U* correction, further accurate predictions of intermolecular interactions and formation energies can be reached[13]. In addition, the *U* correction can further enhance the description of physical properties, other than the electronic structure, including magnetic and structural properties of correlated systems, the electron transfer energetics, and chemical reactions. However, one of the drawbacks of the Hubbard method is that it fails in predicting the properties of systems with more delocalized electrons, such as metals. The relative success of the DFT+U method

is related to its straightforward approach to account for the underestimated electronic interactions by simply adding a semi-empirically tuned numerical parameter "*U*"[12]. This interaction parameter can be easily controlled, making the DFT+U method a tool to give a qualitative assessment of the influence of the electronic correlations on the physical properties of a system.

One of the mostly implemented methods in the DFT+U realm is the LDA+U method. It is widely used due to its simple implementation on the existing LDA codes, which makes it only slightly computationally heavier than the standard DFT computations [14]. In this chapter, we discuss the fundamental formulation of the LDA+U method and examine its applicability for practical implementations for different classes of materials, where DFT is usually found to be impractical. Popular cases of DFT shortage are discussed including materials with strong correlations, defective solid-state materials, and organometallics, while reviewing literature case studies that studied these classes of materials with DFT+U calculations. The methodology of optimizing the *U* correction is inspected, where it can be either formulated from first principles or achieved empirically by tuning the *U* value, while seeking an agreement with experimental results of the system's physical properties. In this chapter, we also present a review of the practical implementation of *U*, while assessing its corrective influence on improving the description of a variety of physical properties related to certain classes of materials. In addition, the effect of the calculation parameters on the chosen *U* value is discussed, including the choice of the localized basis set and the type of DFT functional employed.

2.3.2 Standard DFT Problem

Using exact HF or DFT solutions, the aim is always to reach, as close as possible, the exact description of the total energy of the system. Unluckily, reaching this exact energy description is impossible and approximations have to be employed. In DFT, electronic interaction energies are simply described as the sum of classical Columbic repulsion between electronic densities in a mean field kind of way (Hartree term) and an additive term that is supposed to encompass all the correlations and spin interactions[7]. This additive term, namely the exchange and correlation (xc), is founded on approximations that have the responsibility to recover the exact energy description of the system. This approximated xc functional is a function of the electronic charge density of the system, and the accuracy of a DFT calculation is strongly dependent on the descriptive ability of this functional of the energy of the system[8]. It is generally difficult to model the dependence of the xc functional on electronic charge density, and thus, it can inadequately represent the many-body features of the N-electron ground state. For this reason, systems with physical properties that are controlled by many body electronic interactions (correlated systems) are poorly described by DFT calculations. For these systems, incorrect description of the electronic structure induces the so-called "bandgap problem," which in turn, imposes difficulties in utilizing DFT to predict accurate intermolecular interactions, formation energies, and transition states[14].

The problem of DFT to describe correlated systems can be attributed to the tendency of xc functionals to over-delocalize valence electrons and to over-stabilize metallic ground states[12,13]. That is why DFT fails significantly in predicting the properties

of systems whose ground state is characterized by a more pronounced localization of electrons. The reason behind this delocalization is rooted to the inability of the approximated xc to completely cancel out the electronic self-interaction contained in the Hartree term; thus, a remaining "fragment" of the same electron is still there that can induce added self-interaction, consequently inducing an excessive delocalization of the wave functions[13]. For this reason, hybrid functionals were formulated to include a linear combination of a number of xc explicit density and HF exact exchange functionals, that is self-interaction free, by eliminating the extra self-interaction of electrons through the explicit introduction of a Fock exchange term. However, this method is computationally expensive and is not usually practical when larger, more complex systems are studied. Nonetheless, HF method, which describes the electronic structure with variationally optimized single determinant, cannot describe the physics of strongly correlated materials such as the Mot insulators. In order to describe the behavior of these systems, full account of the multideterminant nature of the N-electron wave function and of the many-body terms of the electronic interactions is needed[12]. Therefore, it is predicted that applying DFT calculations using approximate xc functionals, such as LDA or GGA, will poorly describe the physical properties of strongly correlated systems.

2.3.3 Mot insulators and the Hubbard model

According to the conventional band theories, strongly correlated materials are predicted to be conductive, while they show insulating behavior when experimentally measured. This serious law of the band theory was pointed out by Sir Nevil Mot, who

emphasized that interelectron forces cannot be neglected, which lead to the existence of the bandgap in these falsely predicted conductors (Mot insulators)[15]. In these "metal-insulators," the bandgap exists between bands of like character i.e., between sub-orbitals of the same orbitals, such as 3d character, which originates from crystal field splitting or Hund's rule. The insulating character of the ground state stems from the strong Coulomb repulsion between electrons that forces them to localize in atomic- like orbitals (Mot localization). This Coulomb potential, responsible for localization, is described by the term "*U*," and when electrons are strongly localized, they cannot move freely between atoms and rather jump from one atom to another by a "hopping" mechanism between neighbor atoms, with an amplitude *t* that is proportional to the dispersion (the bandwidth) of the valence electronic states. The formation of an energy gap can be settled as the competition between the Coulomb potential *U* between 3d electrons and the transfer integral *t* of the tight-binding approximation of 3d electrons between neighboring atoms. Therefore, the bandgap can be described by the *U*, *t* and an extra z term that denotes the number of nearest neighbor atoms as[13]:

$$E_{gap} = U - 2zt \qquad (2.15)$$

Since the problem is rooted down to the band model of the systems, alternative models have been formulated to describe the correlated systems. One of the simplest models is the "Hubbard" model[2]. The Hubbard model is able to include the so-called "on-site repulsion," which stems from the Coulomb repulsion between electrons at the same atomic orbitals, and can therefore explain the transition between the conducting and insulating behavior of these systems. Based on this model, new Hamiltonian can be

formulated with an additive Hubbard term that explicitly describes electronic interactions. The additive Hubbard Hamiltonian can be written in its simplest form as follows[13]:

$$Hub = t \sum_{(i,j),\sigma} (c_{i,\sigma}^{\dagger} c_{i,\sigma} + h.c.) + U \sum_{i} n_{i\uparrow} n_{i\downarrow} \qquad (2.16)$$

As predicted, the Hubbard Hamiltonian should be dependent on the two terms *t* and *U*, with <i.j> denoting nearest-neighbor atomic sites and $c^{\dagger}$, c, and n are electronic creation, annihilation, and number operators for electrons of spin on site *i,* respectively. The hopping amplitude *t* is proportional to the bandwidth (dispersion) of the valence electrons, while the on-site Coulomb repulsion term *U* is proportional to the product of the occupation numbers of atomic states on the same site. The system's insulating character develops when electrons do not have sufficient energy to overcome the repulsion potential of other electrons on neighbor sites, i.e., when $t \ll U$. The ability of the DFT scheme to predict electronic properties is fairly accurate when $t \gg U$, while for large *U* values, DFT significantly fails the HF method, which describes the electronic ground state with a variationally optimized single determinant, that cannot capture the physics of Mot insulators.

2.4 The Hubbard Correction

Inspired by the Hubbard model, DFT+U method is formulated to improve the description of the ground state of correlated systems. The main advantage of the DFT+U method is that it is within the realm of DFT, thus does not require significant effort to be implemented in the existing DFT codes and its computational cost is only slightly higher

than that of normal DFT computations. This "*U*" correction can be added to the local and semilocal density functionals offering LDA+U and GGA+U computational operations. The basic role of the *U* correction is to treat the strong on-site Coulomb interaction of localized electrons with an additional Hubbard-like term. The Hubbard Hamiltonian describes the strongly correlated electronic states (*d* and *f* orbitals), while treating the rest of the valence electrons by the normal DFT approximations. For practical implementation of DFT+U in computational chemistry, the strength of the on-site interactions is described by a couple of parameters: the on-site Coulomb term *U* and the site exchange term *J*. These parameters "*U* and *J*" can be extracted from *ab initio* calculations, but usually are obtained semi empirically. The implementation of the DFT+U requires a clear understanding of the approximations it is based on and a precise evaluation of the conditions under which it can be expected to provide accurate quantitative predictions[12,13].

The LDA+U method is widely implemented to correct the approximate DFT xc functional. The LDA+U works in the same way as the standard LDA method to describe the valence electrons, and only for the strongly correlated electronic states (the *d* and *f* orbitals), the Hubbard model is implemented for a more accurate modeling. Therefore, the total energy of the system (E_{LDA+U}) is typically the summation of the standard LDA energy functional (E_{Hub}) for all the states and the energy of the Hubbard functional that describes the correlated states. Because of the additive Hubbard term, there will be a double counting error for the correlated states; therefore, a "double-counting" term (E_{dc}) must be deducted from the LDA's total energy that describes the electronic interactions in a mean field kind of way[12].

$$E_{LDA}+U[\rho(r)]=E_{LDA}[\rho(r)]+E_{Hub}[\{n_{mm}^{I\sigma}\}]-E_{dc}[n^{I\sigma}] \qquad (2.17)$$

Therefore, it can be understood that the LDA+U is more like a substitution of the mean field electronic interaction contained in the approximate xc functional. Nonetheless, the E_{dc} term is not uniquely defined for each system and various formulations can be applied to different systems. The most dominant of these formulations is the FLL formulation[16–18]. It is based on the implementation of fully localized limit (FLL) on systems with more localized electrons on atomic orbitals. The reason for this formulation popularity is due to its ability to expand the width of the Kohn Sham (KS) orbitals and to effectively capture Mot localization. Based on this formulation, the LDA+U can be written as:

$$E_{LDA+U}[\rho(r)]+\sum_{l}[\frac{U^{l}}{2}\sum_{m,\sigma\neq m',\sigma'}n_{m}^{l\sigma}n_{m'}^{l\sigma'}-\frac{U^{l}}{2}n^{l}(n^{l}-1)] \qquad (2.18)$$

where $n_{m}^{l\sigma}$ are the localized orbitals occupation numbers identified by the atomic site index I, state index m and by the spin σ. In equation **(4)**, the right-hand side second and third terms are the Hubbard and double counting terms, specified in equation **(3)**. The dependency on the occupation number is expected as the Hubbard correction is only applied to the states that are most disturbed by correlation effects. The occupation number is calculated as the projection of occupied KS orbitals on the states of a localized basis set:

$$n_{m,m'}^{l\sigma'}=\sum_{k,v}f_{kv}^{\sigma}\left\langle\psi_{kv}^{\sigma}\middle|\varphi_{m}^{I}\right\rangle\left\langle\varphi_{m}^{I}\middle|\psi_{kv}^{\sigma}\right\rangle \qquad (2.19)$$

where the coefficients f_{kv}^{σ} represent the occupations of KS states (labeled by k-point, band, and spin indices), determined by the Fermi-Dirac distribution of the corresponding single-

particle energy eigenvalues. According to this formulation, the fractional occupations of localized orbitals is reduced, while assisting the Mott localization of electrons on particular atomic states[12].

Although the above approach- described in equation **(4.5)** - is able to capture Mott localization, it is not invariant under rotation of the atomic orbital basis set employed to define the occupation number of *n* in equation **(5)**. This variation makes the calculations performed unfavorably dependent on the unitary transformation of the chosen localized basis set. Therefore, "Rotationally invariant formulation" is introduced, which is unitary-transformation-invariant of LDA+U[16]. In this formulation, the electronic interactions are fully orbital-dependent, and thus considered to be the most complete formulation of the LDA +U. However, a simpler formulation that preserves rotational invariance, which is theoretically based on the full rotationally invariant formulation, had proved to work as effectively as the full formulation for most materials[17]. Based on the simplified LDA+U form, it has been customary to utilize, instead of the interaction parameter U, an effective U parameter: U_{eff} =U - J, where the "*J*" parameter is known as the exchange interaction term that accounts for Hund's rule coupling. The U_{eff} is generally preferred, because the *J* parameter is proven to be crucial to describe the electronic structure of certain classes of materials, typically those subject to strong spin-orbit coupling.

2.4.1 Solving the CO Adsorption Puzzle with the U Correction

Studying surface chemistry is of great significance for enhancing the overall efficiency of many electrochemical applications[19–21]. In catalysis, for example, understanding the adsorption mechanism of species on catalytic surfaces – mainly electrodes - is essential in order to formulate a design principle for the prefect catalyst that can reach the optimum efficiency for a desired electrochemical process[22–24]. Typically, the adsorption of CO on metal surface is widely acknowledged as the prototypical system for studying molecular chemisorption[25–28]. Despite the extensive experimental studies, grasping the complete theoretical description of the "bonding model" has not yet been reached, due to the inability of experimental tools to fully describe the details of molecular orbital interactions and to make a profound population analysis, which is based on studying the electronic structures of the substrate and surface particles [31, 32]. To this end, DFT can be utilized to explicitly describe electronic structures of the system particles in greater details, which can help in extending the conceptual model of CO chemisorption [33–38]. Unfortunately, due to the inherent wrong description of the electronic structure by DFT, wrong predictions of CO preferred adsorption sites are observed that contradict experimental results, especially for the (111) surface facets of transition metals, leading to the so called "CO Adsorption *Puzzle*" [29–31]. The root of this DFT problem resides on the fact that both local density and generalized gradient approximation functionals underestimate the CO bandgap, predicting wrong positions of the CO frontier orbitals, which results in an overestimated bond strength between the substrate and surface molecules[32].

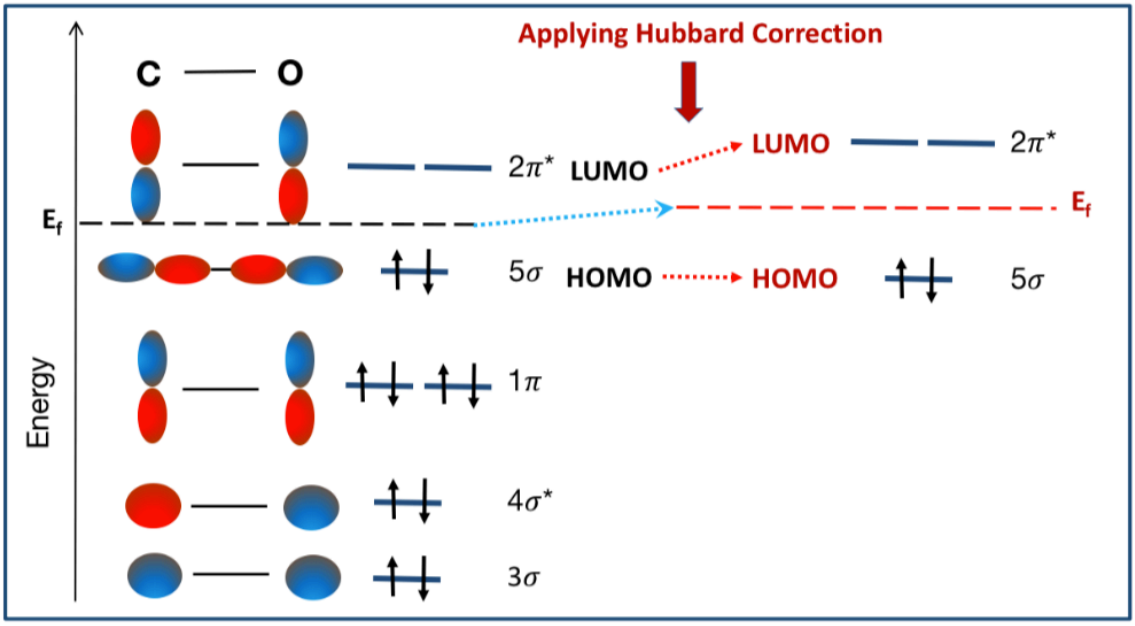

Figure 6. Schematic sketch of the molecular eigen-states of the CO molecule. The DFT + U technique shifts the LUMO orbitals to higher energies, but the energies of the occupied orbitals remain the same.

One of the popular solutions that has been exploited by researchers to resolve the adsorption site prediction puzzle is the DFT+U correction[32,33]. In this approach, the position of the 2π* orbital is shifted to higher values, by adding the on- site Coulomb interaction parameter. By doing so, the interaction of CO 2π* orbital with the metallic *d*-band will no longer be overestimated, bringing the appropriate estimation of the CO adsorption site. Kresse *et al*.[34] first implemented this method, and successfully obtained a site preference in agreement with experiment, emphasizing that the use of such a simple empirical method is able to capture the essential physics of adsorption. DFT calculations utilizing GGA functionals predict adsorption on the three fold hollow-site for Cu(111) and in the bridge-site on Cu(001), instead of the experimental on-top site preference. Reference[33] implanted Kresse's method to investigate the adsorption of CO on Cu(111) and (001) surfaces with 1⁄4 monolayer (ML) coverage on different adsorption sites. In that

study, the HOMO-LUMO gap of the isolated CO molecule was demonstrated to be increased by increasing the value of U. Also, upon changing the U value, the corresponding adsorption energies of the CO over the different adsorption sites were calculated.

Reviewing the Cu(111) surface results, 5 different U values (0.0, 0.5, 1.0, 1.25 and 1.5 eV) were used in the calculations. It was observed that only 20 meV changes in the adsorption energy (higher coordinated hollow sites) for U = 1.25 eV and 0.03 eV for U = 1.5 eV. Nonetheless, the absolute value of adsorption energy decreases linearly with increasing U, where the rate of reduction is found to be larger for higher coordinated sites. It was observed that the site-preference between top and bridge sites to be reversed around the U value of 0.05 eV, while between the top and hollow sites around U = 0.45 eV. Concerning the adsorbate (surface) description in the study, the calculated interlayer relaxations were the same as that calculated using the GGA (PW91) functional without the U correction. Not only does the U correction help in solving the adsorption puzzle dilemma, but it can also enhance the description of other related properties, such as the calculated work function and the vibrational spectra for the CO- metal complexes.

References

1. Griffiths, D. *Introduction to Quantum Mechanics*. *Physical review letters* (2010). doi:10.1119/1.18098
2. Bruus, H. & Flensberg, K. Many-body quantum theory in condensed matter physics: an introduction. (2010).
3. Atkins, P. W. & Friedman, R. *Molecular Quantum Mechanics*. *Oxford Universiy Press* (2011).
4. SHOLL, D. S. & STECKEL, J. A. *Density functional theory: A Practical Introduction*. *John Wiley & Sons, Inc.* **68,** (2009).
5. Groß, A. *Theoretical surface science: A microscopic perspective*. *Theoretical Surface Science: A Microscopic Perspective* (2009). doi:10.1007/978-3-540-68969-0
6. Burke, K. The ABC of DFT. *QMBook* (2004). doi:10.1017/CBO9781107415324.004
7. Koch, W. & Holthausen, M. *A Chemist's Guide to Density Functional Theory, 2nd Edition*. *Wiley-VCH* (2001). doi:10.1002/3527600043
8. Mattsson, A. E., Schultz, P. A., Desjarlais, M. P., Mattsson, T. R. & Leung, K. Designing meaningful density functional theory calculations in materials science—a primer. *Model. Simul. Mater. Sci. Eng.* (2005). doi:10.1088/0965-0393/13/1/R01
9. Geerlings, P., De Proft, F. & Langenaeker, W. Conceptual Density Functional Theory. *Chem. Rev.* (2003). doi:10.1021/cr990029p
10. Kohn, W., Becke, A. D. & Parr, R. G. Density Functional Theory of Electronic

Structure. *J. Phys. Chem.* (1996). doi:10.1021/jp960669l

11. Seidl, A., Görling, A., Vogl, P., Majewski, J. & Levy, M. Generalized Kohn-Sham schemes and the band-gap problem. *Phys. Rev. B - Condens. Matter Mater. Phys.* (1996). doi:10.1103/PhysRevB.53.3764

12. Himmetoglu, B., Floris, A., De Gironcoli, S. & Cococcioni, M. Hubbard-corrected DFT energy functionals: The LDA+U description of correlated systems. *International Journal of Quantum Chemistry* (2014). doi:10.1002/qua.24521

13. Cococcioni, M. The LDA+U Approach: A Simple Hubbard Correction for Correlated Ground States. in *Autumn School on Correlated Electrons, Jülich* **2,** 1–40 (Julich, 2012).

14. Kryachko, E. S. Density Functional Theory and Molecular Interactions: Dispersion Interactions. *Struct Bond* **150,** 65–96 (2013).

15. Anisimov, V. I., Zaanen, J. & Andersen, O. K. Band theory and Mott insulators: Hubbard U instead of Stoner I. *Phys. Rev. B* **44,** 943–954 (1991).

16. Liechtenstein, A. I., Anisimov, V. I. & Zaanen, J. Density-functional theory and strong interactions: Orbital ordering in Mott-Hubbard insulators. *Phys. Rev. B* **52,** (1995).

17. Dudarev, S., Botton, G., Savrasov, S., Humphreys, C. & Sutton, A. Electron-energy-loss spectra and the structural stability of nickel oxide: An LSDA+ U study. *Phys. Rev. B* **57,** 1505–1509 (1998).

18. Anisimov, V. I., Aryasctiawan, F. & Lichtenstein, A. I. First-principles calculations of the electronic structure and spectra of strongly correlated systems : the LDA + U method. *J. Phys. Condens. Matter* **767,** 767–808 (1997).

19. Wang, Y., Wu, G., Yang, M. & Wang, J. Competition between Eley-Rideal and Langmuir-Hinshelwood pathways of CO oxidation on Cun and CunO (n = 6, 7) clusters. *J. Phys. Chem. C* **117,** 8767–8773 (2013).

20. Akhade, S. A., Luo, W., Nie, X. & Bernstein, N. J. Poisoning effect of adsorbed CO during CO 2 electroreduction on late transition metals †. *Phys. Chem. Chem. Phys.* **16,** 20429–20435 (2014).

21. Abbas, A. *et al.* An overview of CO2 electroreduction into hydrocarbons and liquid fuels on nanostructured copper catalysts. *Green Chem. Lett. Rev.* **9,** 166–178 (2016).

22. Chen, M. S. *et al.* Highly active surfaces for CO oxidation on Rh, Pd, and Pt. *Surf. Sci.* **601,** 5326–5331 (2007).

23. Kortlever, R., Shen, J., Schouten, K. J. P., Calle-Vallejo, F. & Koper, M. T. M. Catalysts and Reaction Pathways for the Electrochemical Reduction of Carbon Dioxide. *J. Phys. Chem. Lett. Kortlever R, Shen J, Schouten KJP, Calle-Vallejo F, Koper MTM. Catal. React. Pathways Electrochem. Reduct. Carbon Dioxide. J Phys Chem Lett. 2015;6(20)4073–82.* **6,** 4073–4082 (2015).

24. Nakao, K. *et al.* CO oxidation on Pd(111), Pt(111), and Rh(111) surfaces studied by infrared chemiluminescence spectroscopy. *Surf. Sci.* **601,** 3796–3800 (2007).

25. Sung, S. S. & Hoffmann, R. How Carbon Monoxide Bonds to Metal Surfaces. *J. Am. Chem. Soc.* **107,** 578–584 (1985).

26. Froitzheim, H., Hopster, H., Ibach, H. & Lehwald, S. Applied Physics Adsorption Sites of CO on Pt (1il). **151,** 147–151 (1977).

27. Aizawa, H. & Tsuneyuki, S. First-principles study of CO bonding to Pt(111):

validity of the Blyholder model. *Surf. Sci. Lett.* **399,** L364–L370 (1998).

28. Andersson, S. & Pendry, J. B. Structure of CO adsorbed on Ni(100). *Surf. Sci.* **71,** 75–86 (1978).

29. Feibelman PJ. *et al.* The CO / Pt (111) Puzzle. *J. Phys. Chem. B* (2001).

30. Schimka, L. *et al.* Accurate surface and adsorption energies from many-body perturbation theory. *Nat. Mater.* **9,** 741–744 (2010).

31. Stroppa, a, Termentzidis, K., Paier, J., Kresse, G. & Hafner, J. CO adsorption on metal surfaces: a hybrid functional study with plane wave basis set. *Phys. Rev. B* **76,** 32 (2007).

32. Mason, S. E., Grinberg, I. & Rappe, A. M. First-principles extrapolation method for accurate CO adsorption energies on metal surfaces. *Phys. Rev. B - Condens. Matter Mater. Phys.* **69,** (2004).

33. Gajdos, M. & Hafner, J. CO adsorption on Cu(111) and Cu(001) surfaces: improving site preference in DFT calculations. (2004). doi:10.1016/j.susc.2005.04.047

34. Kresse, G., Gil, A. & Sautet, P. Significance of single-electron energies for the description of CO on Pt(111). *Phys. Rev. B - Condens. Matter Mater. Phys.* **68,** (2003).

Chapter 3

Literature Survey

The CO adsorption on transition metal surfaces show fascinating complexities; it may adopt one-fold (atop), two-fold (bridge), or three-fold or four-fold (hollow) coordination sites depending of a number of parameters, including: type of the substrate material, the kind of surface, and the surface coverage[1]. For example, CO thermodynamically prefers to adsorb ontop sites at all Cu surfaces, whereas CO preference changes with the change of the surface facets for Ni; preferring atop-site at Ni(100), the bridge-site at the Ni(110), and the hollow-site at the Ni(111)[1]. The different measured relative energetics at these sites are interpreted by the electronic structures. DFT calculations, however, were able to reproduce experimental findings correctly at particular surfaces, while incorrectly predicting energetics at other surfaces that resulted in wrong site-preference predictions. However, if the limitations of computational theories are understood, they can be exploited to provide quantitative structural information that can considerably help in extending the conceptual model of the CO adsorption.

3.1 The CO Chemisorption Model

The Blyholder model frontier orbitals two-step bonding process is a rather simple yet not complete description of the bonding mechanism. Previous work by Fohlisch *et al*[2–4] had refined the Blyholder model showing a contribution of the 1π, 2π*, 4σ and 5σ orbitals with the metal d-states and verified a full orbital mixing of the CO σ- and π-orbitals. Stroppa *et al*[5] further refined the model by verifying the contribution of the broad metal *sp*

states in the interaction by their hybridization with the CO σ- and π-orbitals. Our electronic structure and charge distribution results support these claims and verify the contribution of all metallic states and CO orbitals with different magnitudes, depending on their respective energy levels and geometrical positioning. Furthermore, the depiction of orbitals other than the frontier (5σ and 2π*) orbitals is rather essential for interpreting the discrepancies in the charge transport and the adsorbate final geometry results, which are found when the adsorption at the same adsorption site on different surface facets is compared. Several later models confirmed the hybridization of all the initial orbitals of the CO molecule. Orbital mixing between the CO 5σ and 4σ were noticed from both experimental and theoretical studies, based on a detailed orbital interaction and its energetics studies [3,6,7]. In addition, the attractive nature of the 5σ interaction was criticized and a rather repulsive nature is

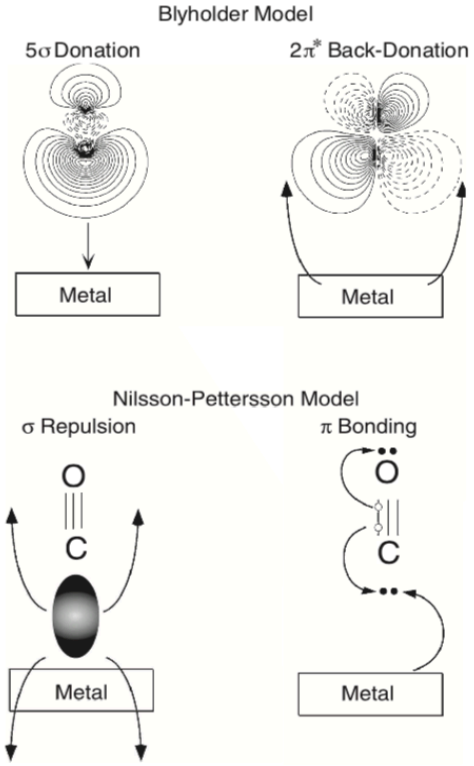

extensively discussed by Bagus *et al*[8,9]. Regarding the nature of the CO π-orbitals, later studies confirmed a perturbation of the complete π -orbital framework upon adsorption, where the hybridization between the 1π, 2π*, and the metallic d_π - orbitals is experimentally observed, in agreement with the original Blyholder model.

A more accurate description of the orbitals interactions became only possible in the early 2000s, after the application of the X-ray emission spectroscopy (XES) in the adsorbate electronic structure investigations. XES allows for an atom- and symmetry projected analysis of the adsorbate valence states. Fohlisch *et al* exploited experimental XES technique along with *ab initio* DFT calculations to test the validity of the original Blyholder model and the later Frontier orbital descriptions of the adsorption mechanism. Based on their rigorous electronic structure investigations, the new Blyholder-Nilsson-Petersson (BNP) model was proposed, which provides a more complete molecular orbital picture of the adsorption mechanism. The BNP model rather claims the hybridization of both the σ and π orbitlas of the CO molecule. Using XES, π and σ systems were allowed to be studied independently. In both the π- and σ- systems, full hybridization of the participating molecular orbitals was observed. In the π -system, the simple 2π* back-donation picture agreed with the observed XE spectral results at π -symmetry. For the 2π* back-donation to be confirmed, the 2π* orbitals were expected to largely polarize towards the C end, however, the contrary was observed and the 2π* orbital rather polarized towards the oxygen atom. In addition, the repulsive nature of the σ-interaction was confirmed by the observed depopulation of the whole s-system, including the 4σ, 5σ, and the *d* orbitals with σ symmetry (d_σ) orbitals, where orbitals are depleted to minimize the repulsion. Based on these observations, the adsorption energetics were concluded declaring an attractive

(stabilizing) π -interactions that is compensated with a repulsive (destabilizing) σ interaction. The balance between the stabilizing and destabilizing interactions explains the measured weak substrate-adsorbate bonding. Regarding the CO molecule, the internal C-O bond carried by π -interaction is found to be weakened upon adsorption, whereas the bond carried by σ-interaction is strengthened.

In the following section we are going to survey the experimental methods utilized to draw the most updated model, which is the Nilsson-Petersson Model.

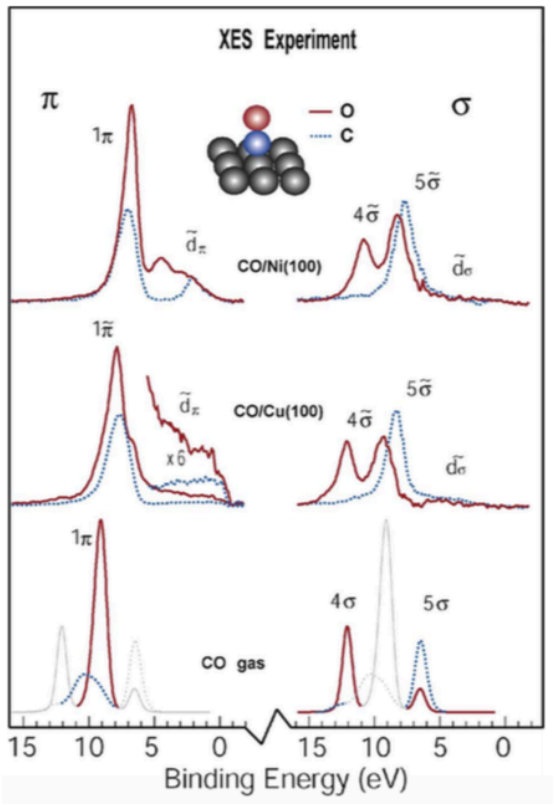

3.2 The Nilsson-Petersosn Model

The molecular orbital picture of the chemisorption process is mainly drawn from the electronic structure data coming from the XES spectra. Figure 8 shows the XES spectra for the π and σ systems. Since XES enables us to study each system independently, we are going to begin with analyzing the π-system and then dwell into the σ-system.

3.2.1 The π-system

From the π- symmetry XE results in Figure 8, we observe a dominant 1π state for the chemisorbed CO for both C and O XE spectra. New states are observed towards lower binding energies, which differ in O and C spectra; these new states are denoted as the dπ band. At the bottom of the dπ band, i.e. at higher binding energies, we observe intensity only in the O spectrum, which is denoted as a lone-pair state of π-symmetry at 4.5 eV. Close to the Fermi level (at the top of the band), intensity becomes present in both C and O spectra. Upon adsorption, the 1π forms a bonding combination to the metal *d*-orbitals, where the overlap is maximized through internal polarization. Next, we are going to study the orbital contour plots in order to gain more insights about orbitals polarizations (*Figure 9*)

From the orbital plots we can observe the 1π becoming more polarized towards C in comparison with the free molecule. Simultaneously, a lone pair state is formed on the outer atom with large Ni *d*-character. Upon adsorption, the 2π* polarized towards the O atoms, which is opposite to the 1π polarization towards the C end. Thus, we have the so-called orbital rotation between the 1π and 2π* orbitals. At the bottom of the *d*-band ($d_{\pi\text{-b}}$)

the nodal plane coincides with the carbon atom forming the oxygen lone-pair. As we go to the top of the band ($d_{\pi\text{-t}}$), the nodal plane becomes more located between the C and O atoms[4].

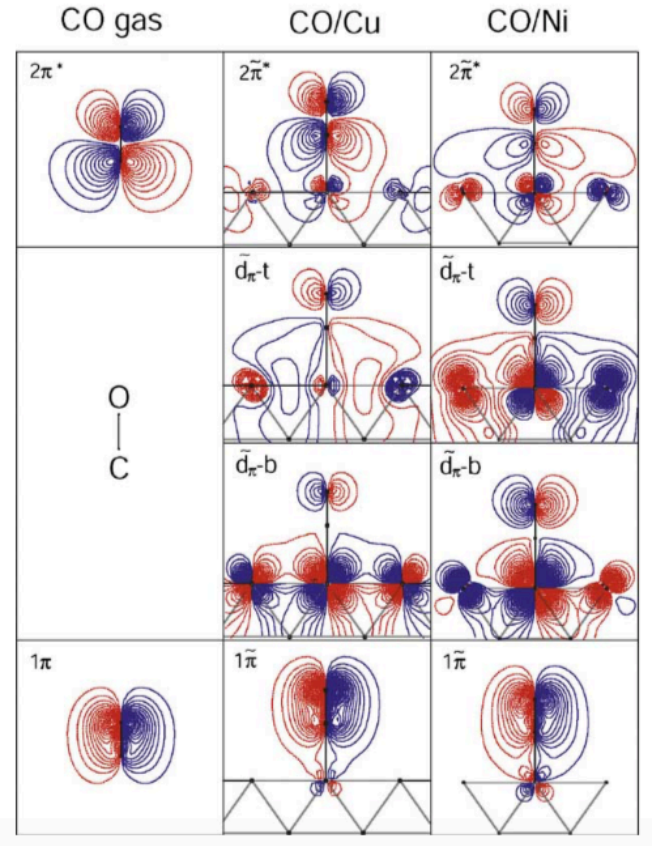

3.2.2 The σ-system

Investigating *Figure 8* XE spectrum of σ-symmetry we can observe the 4σ five times larger than the 5σ. It's worth-noting that the relative strength of the 4σ and 5σ in the O XES after adsorption is a measure of the degree of polarization. Upon adsorption, the 4σ becomes even weaker than the 5σ, where both the peaks of the 4σ and 5σ orbitals deviate

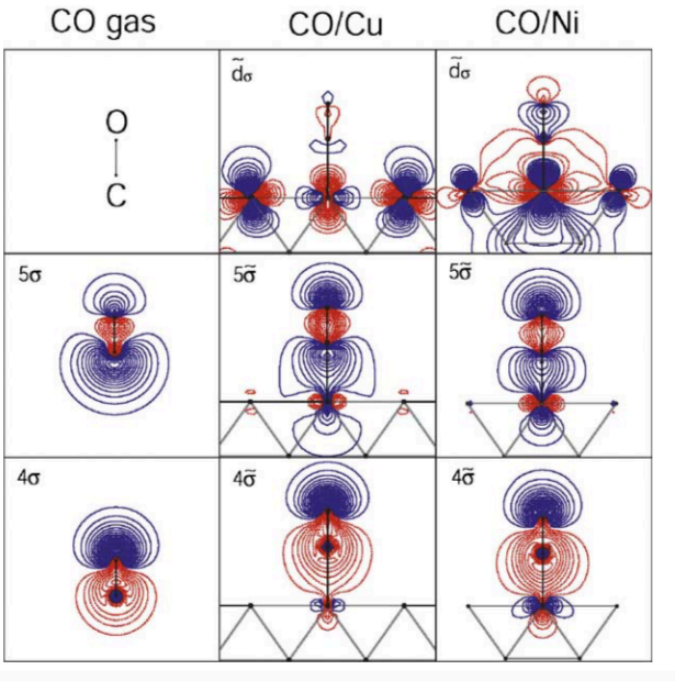

Figure 10. Contour plots for CO σ-orbitals in the gas phase and adsorbed on Ni13 and Cu26 clusters. Different colored lines denote different phases of the wave-functions.[1]

from their original energy positions in the free CO molecule. The upshift of the 5σ to higher binding energies was interpreted as a sign of attractive 5σ dative bonding[10–14], however, the correct interpretation for this is that the entire σ system show internal redistribution so that it can minimize the adsorbate-metal repulsion[1,3]. This interpretation is evidenced by the polarization of the 5σ away from the C atom and towards the O atom, where it changes character from antibonding to bonding, leading to a higher binding energy. This is clearly elaborated in the orbital plots in *Figure 10*

3.2.3 Charge Density Difference Analysis

From total plot in the uppermost figure of the total charge density difference plots in *Figure 11*, we can observe a loss and gain of charge in all atomic centers. There also

seem a small gain in charge between Ni and C. The small gain has been discussed in terms of electron pair creation due to the suggested σ donation. In addition, there also seems to be a gain of charge in the π-symmetry, which supports the back-bonding idea into the 2π* orbitals. Theoretically, however, it is possible to calculate charge densities of the π and σ systems individually. In the charge density difference plot of the σ-symmetry, we can observe the entire σ-system, including the d_σ orbitals, losing charge upon adsorption[1]. This depopulation of σ- and *d*-orbitals occurs in order to minimize the repulsion. Since the depopulation involves the 3d and 4s orbitals of the Ni atoms, the Ni-Ni bonds get weakened

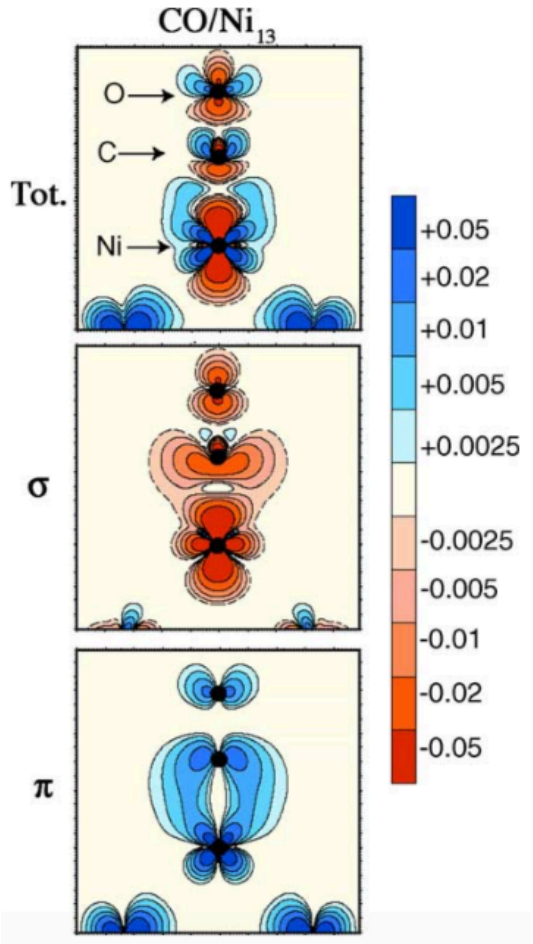

as a consequence of the interaction with the CO molecule. On the other hand, the entire π-system gains charge, where the π interaction forms a bonding combination between the CO 2π* and the Ni 3d orbitals. It is also revealed that the 2π* becomes populated by 22%, whereas the 1π gets depopulated by 10%, giving a net gain of 10% population in the π-system[1,4].

3.3 Gap in Research and Thesis Approach

The adsorption mechanism is solely controlled, and thus described, by the electronic interaction between the substrate atoms and the adsorbing molecule[15,16]. Different adsorption mechanisms take place depending on the thermodynamically preferable adsorption site(s)[17–19]. For each adsorption site, unique changes for both the substrate and the adsorbed molecule take place, including changes in the electronic, vibrational, charge distribution, and structural properties[20–23]. Predicting these changes for the adsorbed molecule is critical for the study of catalytic behavior of different materials[24–27]. Based on the required changes that occur upon interaction, innovative design principles of materials to be used in a wide range of applications can be realized[28,29].

Density functional theory (DFT) is an ideal computationally convenient method for generating the required detailed electronic structure for describing the CO adsorption process[30]. However, DFT may fail to describe the correct position of energy levels for the studied system resulting in wrong energetics calculations, and consequently, wrong site preference for the CO molecule[31,32]. This problem is manifested in the CO adsorption on the (111) transition metal surface facets, often referred to as the CO adsorption puzzle[33,34].

The root of this DFT problem resides on the fact that both local density and generalized gradient approximation functionals fail to predict the correct positions of the CO frontier orbitals, 5σ (HOMO) and 2π* (LUMO). These orbitals are located closer to the fermi level, making the 2π* orbital very close in energy to the metal d-band, which results in an overestimated bond strength of the 2π*-d-band bonding interaction[35]. In addition, because of their open d-shells and accompanying spin-coupling, near-degeneracy and dynamical correlation problems, predictions of the electronic structure of transition metal surfaces presents another challenge for theoretical calculations. Consequently, most semi-local exchange-correlation (xc) density functionals underestimate surface energies and predict them more stable than they actually are. Different approaches were employed to solve the puzzle, either by manually shifting the CO bandgap using the DFT+U approach[31,36,37], or by utilizing expensive hybrid functional calculations[16,38,39]. However, despite the more accurate CO bandgap description by hybrid functionals, the correct site preference on (111) surfaces was not possible for open d-shell transition metals and was only correct for metals with closed d-shell configuration, such as Cu, making it an ideal choice for open d-shell transition metals. Therefore, additional factors, other than the accuracy of the frontier orbital energy description, must be considered for a better understanding of the adsorption puzzle.

For pure DFT calculations without corrections, in the study done by Schimka *et al*[35], it was shown that density functionals with low or no gradient corrections predicted reasonable surface energies, while vastly overestimating their bond strengths. This bond overestimation is logical, because of the previously stated CO 2π* orbital downshift error.

On the other extreme, for semi- local functionals with strong gradient corrections, surface energies were found to be overly-stabilized, however, the adsorption energies predictions were considerably improved. This improvement in adsorption energetics can be interpreted as a cancelation of error by making the surface artificially more stable using strong gradient functionals to counteract the over- strengthened adsorption bond. Therefore, for the purpose of studying surface interactions, a computationally convenient shortcut is to employ a density functional with strong gradient corrections - in our case RPBE - to obtain accurate energetics results. It is worth-mentioning, though, that incorrectly predicting site preferences do not necessarily imply poor description of surface chemical phenomena[40], which is also proved in our results, where the heat of adsorption is found to act as sole descriptor for the site preference, without interfering with the mechanism of adsorption at different sites.

3.3.1 Thesis Approach

Herein, insights on the arrangement of surface atoms as an overlooked parameter that extensively contributes to the surface bonding mechanism were demonstrated, which in turn constitutes the adsorption thermodynamics and the preferred adsorption site. Within the present investigation, the reliability of DFT calculations for the description of surface interactions is validated, despite the expected inaccurate energetics and site preference calculations. We further exploit the inaccurate frontier orbital energy description to explain the resulting contradicting site preferences. To investigate the effect of both the surface type and adsorption site on the adsorption mechanism and energetics, a comprehensive

DFT study for CO adsorption on all available adsorption sites over distinctive surface facets, (100), (110), and (111) surfaces[10,41,42] is presented. At each surface and for each site, adsorption mechanisms are analyzed from molecular orbital and charge transport principles. This comparison is also extended by spotting alterations in CO non-frontier orbitals, such as the 3σ and 1π, for similar adsorption sites at different surfaces, which is found essential for understanding alterations caused by varying arrangements of surface atoms.

References

1. Nilsson, A. & Pettersson, L. G. M. Chemical bonding on surfaces probed by X-ray emission spectroscopy and density functional theory. *Surface Science Reports* **55,** 49–167 (2004).

2. Föhlisch, a. *et al.* Ground-state interpretation of x-ray emission spectroscopy on adsorbates: CO adsorbed on Cu(100). *Phys. Rev. B* (2000). doi:10.1103/PhysRevB.61.16229

3. Föhlisch, A. *et al.* How carbon monoxide adsorbs in different sites. *Phys. Rev. Lett.* **85,** 3309–3312 (2000).

4. Föhlisch, A. *et al.* The bonding of CO to metal surfaces. *J. Chem. Phys.* **112,** 1946–1958 (2000).

5. Stroppa, a, Termentzidis, K., Paier, J., Kresse, G. & Hafner, J. CO adsorption on metal surfaces: a hybrid functional study with plane wave basis set. *Phys. Rev. B* **76,** 32 (2007).

6. Hu, P., King, D. A., Lee, M. H. & Payne, M. C. Orbital mixing in CO chemisorption on transition metal surfaces. *Chem. Phys. Lett.* **246,** 73–78 (1995).

7. Greuter, F., Heskett, D., Plummer, E. W. & Freund, H. J. Chemisorption of CO on Co(0001). Structure and electronic properties. *Phys. Rev. B* **27,** 7117–7135 (1983).

8. Bagus, P. S., Nelin, C. J. & Bauschlicher, C. W. Bonding of CO to metal surfaces: A new interpretation. *Phys. Rev. B* **28,** 5423–5438 (1983).

9. Bagus, P. S. & Hermann, K. New analysis of lone-pair binding-energy shifts in photoemission from adsorbed molecules: CO and NH3 on Cu(100). *Phys. Rev. B* **33,** 2987–2991 (1986).

10. Hammer, B., Hansen, L. B. & Nørskov, J. K. Improved adsorption energetics within density-functional theory using revised Perdew-Burke-Ernzerhof functionals. *Phys. Rev. B - Condens. Matter Mater. Phys.* **59,** 7413–7421 (1999).

11. Sung, S. S. & Hoffmann, R. How Carbon Monoxide Bonds to Metal Surfaces. *J. Am. Chem. Soc.* **107,** 578–584 (1985).

12. Eastman, D. E. & Cashion, J. K. Photoemission energy-level measurements of chemisorbed CO and O on Ni. *Phys. Rev. Lett.* **27,** 1520–1523 (1971).

13. Allyn, C. L., Gustafsson, T. & Plummer, E. W. The chemisorption of CO on Cu(100) studied with angle resolved photoelectron spectroscopy. *Solid State Commun.* **24,** 531–534 (1977).

14. Wimmer, E., Fu, C. L. & Freeman, A. J. Catalytic promotion and poisoning: All-electron local-density-functional theory of CO on Ni(001) surfaces coadsorbed with K or S. *Phys. Rev. Lett.* **55,** 2618–2621 (1985).

15. Gunasooriya, G. T. K. K., Van Bavel, A. P., Kuipers, H. P. C. E. & Saeys, M. CO adsorption on cobalt: Prediction of stable surface phases. *Surf. Sci.* (2015). doi:10.1016/j.susc.2015.06.024

16. Stroppa, a, Termentzidis, K., Paier, J., Kresse, G. & Hafner, J. CO adsorption on metal surfaces: a hybrid functional study with plane wave basis set. *Phys. Rev. B*

76, 32 (2007).

17. Santen, R. van. Coordination of carbon monoxide to transition-metal surfaces. *J. Chem. Soc. Faraday …* **1934,** 1915–1934 (1987).

18. Ding, K. *et al.* Identification of active sites in CO oxidation and water-gas shift over supported Pt catalysts. *Science (80-.).* (2015). doi:10.1126/science.aac6368

19. Surnev, S. *et al.* Unusual CO Adsorption Sites on Vanadium Oxide−Pd(111) "Inverse Model Catalyst" Surfaces. *J. Phys. Chem. B* (2003). doi:10.1021/jp0223408

20. Hao, X., Wang, B., Wang, Q., Zhang, R. & Li, D. Insight into both coverage and surface structure dependent CO adsorption and activation on different Ni surfaces from DFT and atomistic thermodynamics. *Phys. Chem. Chem. Phys.* (2016). doi:10.1039/C6CP01689H

21. Eren, B. *et al.* Activation of Cu(111) surface by decomposition into nanoclusters driven by CO adsorption. *Science (80-.).* (2016). doi:10.1126/science.aad8868

22. Angelucci, C. A., Ambrosio, R. C. & Gewirth, A. A. Origins of Less Noble Behavior by Au during CO Adsorption. *ACS Catal.* (2018). doi:10.1021/acscatal.7b03736

23. Öström, H. *et al.* Probing the transition state region in catalytic CO oxidation on Ru. *Science (80-.).* **347,** (2015).

24. Nie, X., Luo, W., Janik, M. J. & Asthagiri, A. Reaction mechanisms of CO2

electrochemical reduction on Cu(111) determined with density functional theory. *J. Catal.* **312,** 108–122 (2014).

25. Nakao, K. *et al.* CO oxidation on Pd(111), Pt(111), and Rh(111) surfaces studied by infrared chemiluminescence spectroscopy. *Surf. Sci.* **601,** 3796–3800 (2007).

26. Hammer, B. & Norskov, J. K. Theoretical Surface Science and Catalysis — Calculations and Concepts. *Adv. Catal.* (2000). doi:http://dx.doi.org/10.1016/S0360-0564(02)45013-4

27. Loveless, B. T., Buda, C., Neurock, M. & Iglesia, E. CO chemisorption and dissociation at high coverages during CO hydrogenation on Ru catalysts. *J. Am. Chem. Soc.* (2013). doi:10.1021/ja311848e

28. Sharafeldin, I. M. & Allam, N. DFT Insights into the Electronic Properties and Adsorption of NO2 on Metal-Doped Carbon Nanotubes for Gas Sensing Applications. *New J. Chem.* (2017). doi:10.1039/C7NJ03109B

29. Jiawei, W. *et al.* H2O and CO coadsorption on Co (0001): The effect of intermolecular hydrogen bond. *Surf. Sci.* (2017). doi:10.1016/j.susc.2017.04.008

30. Nilsson, A. & Pettersson, L. G. M. Chemical bonding on surfaces probed by X-ray emission spectroscopy and density functional theory. *Surf. Sci. Rep.* (2004). doi:10.1016/j.surfrep.2004.06.002

31. Tolba, S., Gameel, K., Ali, B., Ali, H. & Allam, N. The DFT+U: Approaches, Accuracy, and Applications. in *Density Functional Calculations: Recent Progresses of Theory and Application* (ed. Yang, G.) (IntechOpen, 2018).

doi:10.5772/intechopen.72020

32. Feibelman, P. J. *et al.* The CO/Pt (111) Puzzle. *J. Phys. Chem. B* (2001). doi:10.1021/jp002302t

33. Hu, Q. M., Reuter, K. & Scheffler, M. Towards an exact treatment of exchange and correlation in materials: Application to the ‘cO adsorption puzzle’ and other systems. *Phys. Rev. Lett.* (2007). doi:10.1103/PhysRevLett.98.176103

34. Lazić, P. *et al.* Density functional theory with nonlocal correlation: A key to the solution of the CO adsorption puzzle. *Phys. Rev. B - Condens. Matter Mater. Phys.* **81,** (2010).

35. Schimka, L. *et al.* Accurate surface and adsorption energies from many-body perturbation theory. *Nat. Mater.* **9,** 741–744 (2010).

36. Kresse, G., Gil, A. & Sautet, P. Significance of single-electron energies for the description of CO on Pt(111). *Phys. Rev. B - Condens. Matter Mater. Phys.* **68,** (2003).

37. Gajdoš, M. & Hafner, J. CO adsorption on Cu(1 1 1) and Cu(0 0 1) surfaces: Improving site preference in DFT calculations. *Surf. Sci.* **590,** 117–126 (2005).

38. Stroppa, A. & Kresse, G. The shortcomings of semi-local and hybrid functionals: What we can learn from surface science studies. *New J. Phys.* (2008). doi:10.1088/1367-2630/10/6/063020

39. Zeng, Z. & Greeley, J. Theoretical study of CO adsorption on Au catalysts under

environmental catalytic conditions. *Catal. Commun.* (2014). doi:10.1016/j.catcom.2014.03.016

40. Feibelman, P. J. *et al.* The CO/Pt(111) Puzzle †. *J. Phys. Chem. B* **105,** 4018–4025 (2001).

41. Ma, S. H., Zu, X. T., Jiao, Z. Y. & Zhang, X. Z. A test of empirical correction to site preference: DFT calculations for CO adsorption on Co(0 0 0 1) surface. *J. Mol. Struct. THEOCHEM* **864,** 68–71 (2008).

42. Chen, C. *et al.* High coverage CO adsorption and dissociation on the Co(0001) and Co(100) surfaces from DFT and thermodynamics. *Appl. Catal. A Gen.* **523,** 209–220 (2016).

Chapter 4

Computational Methods

As discussed in chapter 1, DFT and experiment have often been teammates in successful surface science projects. In this section, the methods of applying practical DFT calculations on solid surfaces is displayed and to describe molecular surface interactions.

4.1 Slab Models and Periodic Boundary Conditions

Solid surfaces are treated as a solid-state material that is described by geometrical symmetry that can minimize the number of atoms in the system[1]. The periodicity of the system should be utilized to provide infinite three-dimensions. However, for surfaces, the system is infinite in two dimensions and finite in the third dimension along the surface normal. There are computational codes that apply periodic boundary conditions on two-dimensions only, however most of the codes, and the one used in this thesis project, apply boundary conditions in all three dimensions. The problem with the periodicity of the third dimension along the surface normal can be easily solved by using the vacuum slab trick. As illustrated in *Figure 12*, the supercell presented consist of a five-layer slab with a vacuum space with a specific height that separates the upper surface layer from the lowest surface layer of the repeated slab on the vertical axis along the surface normal. In the "slab model", the super cell is repeated in all three dimensions and the vacuum height is chosen such that the electron density tails off to zero in the vacuum space and the top of the surface slab has no effect on the bottom of the upper next slab.

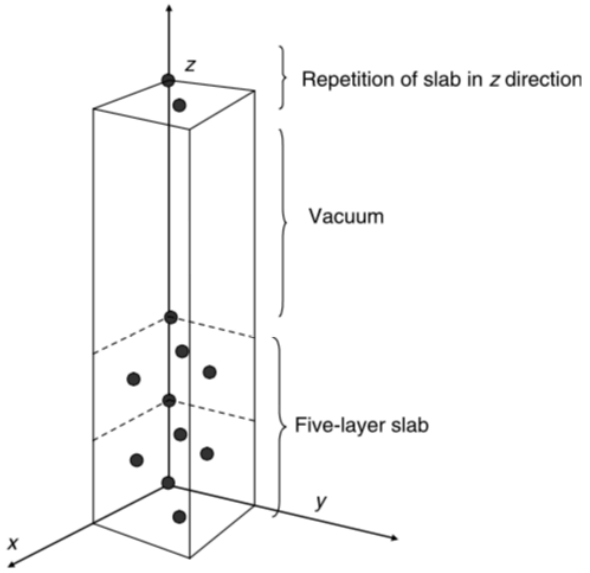

Figure 12. Slab supercell model used for surface energy calculations.[1]

Therefore, the slab model defines a series of stacked solid material separated by vacuum spaces as represented in *Figure 13*.

Intuitively speaking, to ensure no interaction between two neighboring slabs, one can choose a very large vacuum height, however, the bigger the vacuum space the larger the computational cost of your calculation. So, the conventional practice is to find the minimum vacuum space that minimizes the computational requirements and at the same time the space that is enough to make the charge density to keep the charge density inside the vacuum space close to zero[2].

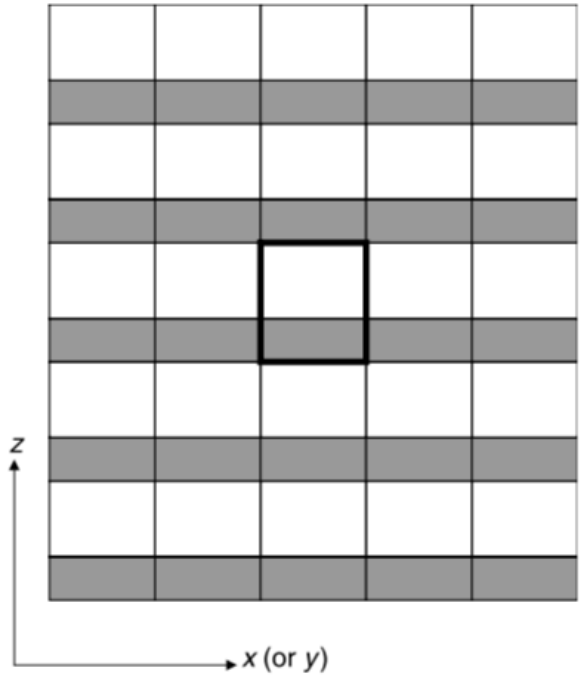

Figure 13. Showing 25 replicas of the original supercell with the bold frame. The grey region indicates the surface thickness, while the white region indicates the vacuum thickness[1].

Realistically, the surface interactions include the upper surface and the bottom layers with a slab thickness of at least microns thick[2], which is far away from any computationally practically large number of layers. So, the larger the number of layers the better your model is. Another way to tackle this problem, the surface energy or the adsorption energy can be tested at different layer thicknesses until there is no more change in the value of the tested property after increasing the slab thickness.

4.2 *K*-point Sampling for Surfaces

For both the bulk and surface models, the Monkhorst – Pack method can be employed for choosing the *k* points for calculations. Since the supercell has a one long

dimension in the direction normal to the surface, in the reciprocal space, there this dimension will be the short dimension. If the vacuum slab is large enough to keep the electron density close to zero a short distance from the edge of the slab, we will then need no more than just one *k* point in the surface normal direction. Therefore, it is convenient to use an MxN x1 *k*-point mesh, where M and N are chosen to adequately sample k space in the plane of the surface[1].

4.3 Surface Relaxation

Since the coordination of the atoms at the surface is reduced compared to the atoms of the bulk, then it is expected that the spacing between the layers near the surface be somewhat different from those in the bulk. This phenomenon is referred to as "Surface Relaxation", and the primary step before carrying any surface calculations is to characterize this relaxation. In ***Figure 14***, on the left side, the original slab model without relaxation with the same spacing between layers is shown, while on the right side, we show the top three layers are allowed to relax, while the bottom three ones are fixed in their positions. The relaxed surface must then have a lower energy than that of the original slab. This relaxation can be reached by performing energy minimization as a function of the positions of the atoms in the slab model. This is done by considering the bottom layers of the supercell as bulk atoms that are constrained to their ideal bulk positions, while the upper layers representing the surface and are allowed free motion in space.

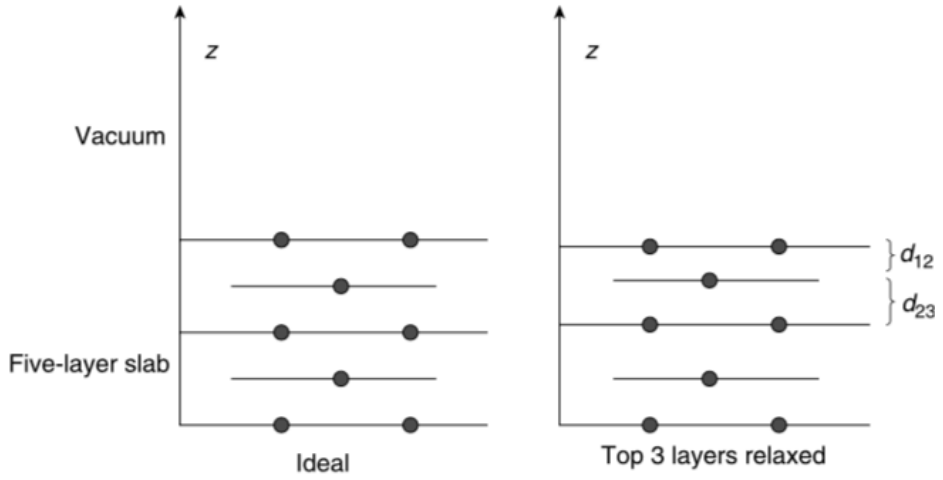

Figure 14. On the left is a schematic of the ideal surface without relaxation; on the right is the relaxed surface with the upper two layers getting constrained[1]

After performing energy minimization, it is usual observe the spacing between the upper three layers getting narrower than that of the bulk. The new spacing is often expressed as a percentage of the original bulk spacing, with negative values indicating contraction and positive values indication expansion.

4.4 Surfaces Classified by Miller Indices

There are many ways in which the bulk can be cleaved into different facets with unique geometrical atomic arrangements. Each way of cleaving the surface is given a specified notation to define how the surface to be cleaved will be defined. The miller indices are defined by the reciprocal of the point of intersection with the axes. For example, the (111) surface cleavage is shown in *Figure 15a*, where the intercepts are at the points (1,1,1) making a triangular surface. Similarly, in *Figure 15c*, the (001) surface is shown, which cuts the z-axis at 1 and is infinite in the other two axes; in this case the reciprocal of

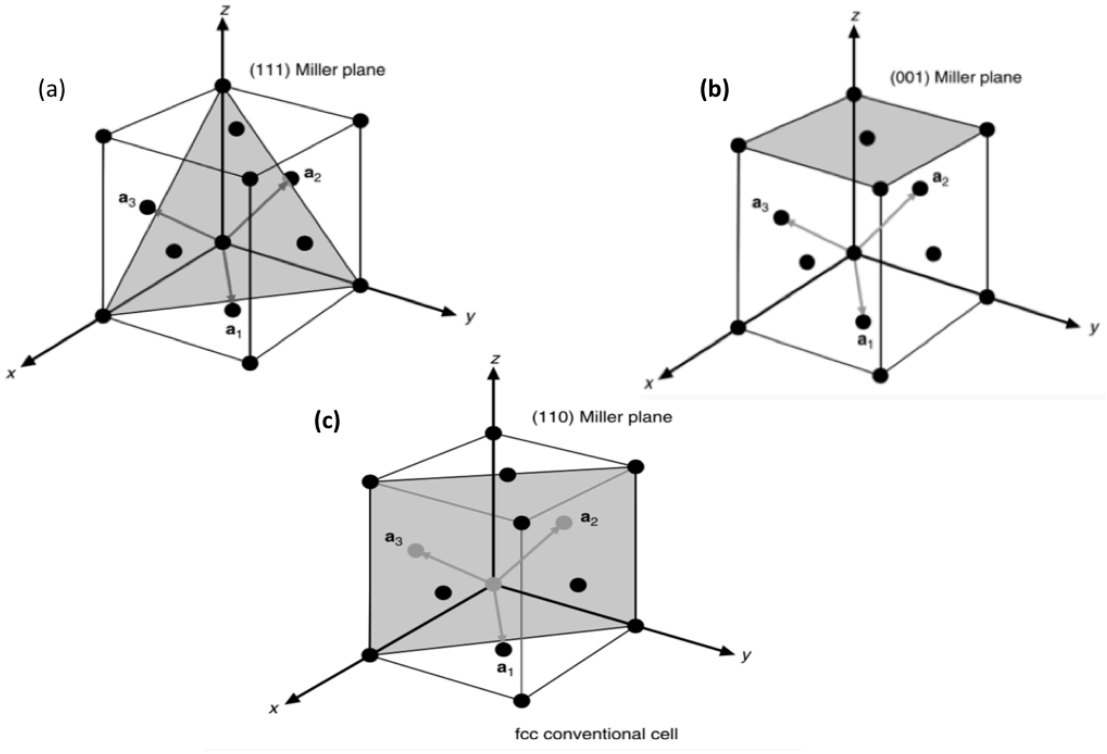

Figure 15. Shows the miller indices notation for surface cleavages that form (a) the (111) surface, (b) the (100), and (c) (110).[1]

these (1/∞, 1/∞, 1/1) gives (0,0,1). Finally, in *Figure 15c* (110) plane, the surface cuts the x and y axes at 1 and is infinite in the z-axis; so, (1/1,1/1,1/∞) will give (110) notation in the Miller indices.

4.5 Applied Surface Computations

In this project, Materials Studio software was for DFT calculations. The calculations were carried out employing the CASTEP computational package.

4.5.1 Optimizing the Bulk Solid Substrate

The first step to applying surface computations is to prepare the bulk structure of the substrate model. One can either build the crystal structure of the bulk by inserting the lattice parameters of the crystal structure of the metal used and the space-group. The bulk crystal structure of Cu is taken in our calculations from the library of solids saved on Materials Studio. The space-group of the Bulk Cu is *FM-3M (255)* with lattice experimental parameters of 3.89 Å. For accelerate the computational time, we took advantage of the symmetry of the FCC crystal structure, and the computations were run on by converting the conventional cell into its primitive form.

The calculated lattice parameters after geometry optimizations is 3.615, which denotes an accuracy of 93%.

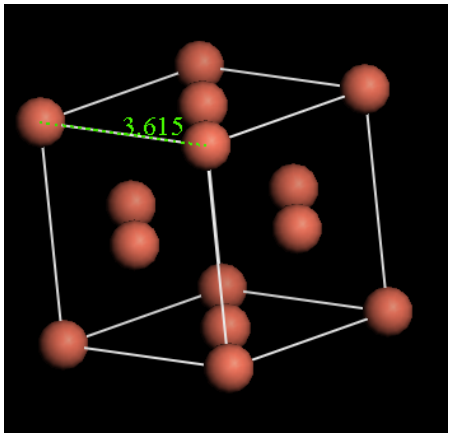

Figure 16. Geometrically Optimized Bulk Cu Crystal

4.5.2 Building and Optimizing the CO molecule

Since the CASTEP package we are using can only work with periodic systems, the CO molecule being a non-periodic system will be dealt with in a special treatment. In order to optimize the CO molecule, we must put it in a crystal structure, so we can exploit the periodicity of the crystal structure for the CASTEP calculations. In this case we build a crystal structure with lattice parameters of 8 Å, which is large enough to ensure no CO-CO interactions vertically or horizontally.

The experimental C-O bond length is 1.1283 Å, while the calculated bond length after optimization is 1.145 Å, which denotes a calculation accuracy of 98.5%.

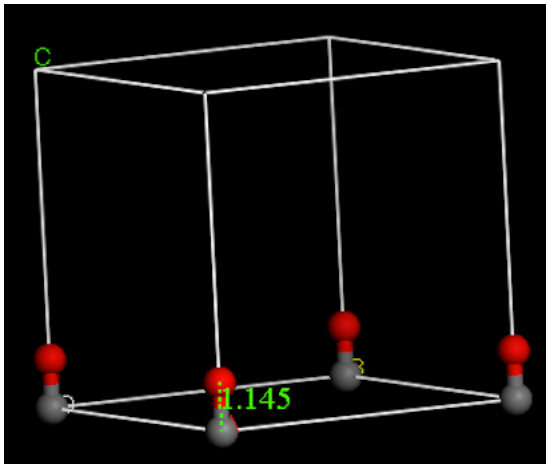

Figure 17. Optimized CO molecule; CO molecules placed at the corners of the crystal with lattice parameters of 8 Å.

4.5.3 Building and Optimizing Surfaces

Figure 18 shows how the (110) surface is cleaved from the bulk of the Pd metal[3]. Using the same method, we cleaved the bulk at the (100), (110), and (111) surfaces. While

cleaving the surface, we choose the slab thickness which constitutes the number of layers we need to model in our slab.

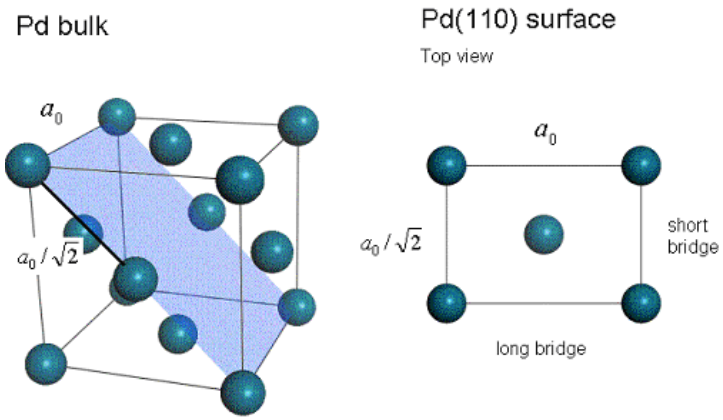

Figure 18. Showing a cleavage of the metal bulk FCC crystal at the (110) plane.[3]

Choosing the Optimum Number of Layers

As previously discussed, the larger the thickness of the surface slab, the more accurate your calculations are, however, on the expense of larger computational requirements. To test for the optimum thickness required for our calculations, we carried out adsorption energy calculations for 3-layers, 4-layers, and 5-layers slab models for the (100) surface to test for the minimum number of layers that can describe the system with the required accuracy. In all cases, the upper two layers were allowed to relax, while the lower surfaces were fixed in their fractional positions.

Although the three surfaces produced different surface energy results, which was expected because of the different number of atoms, when *ontop* adsorption is compared, the most accurate result that is closer to experiment was found at the 3-layer system.

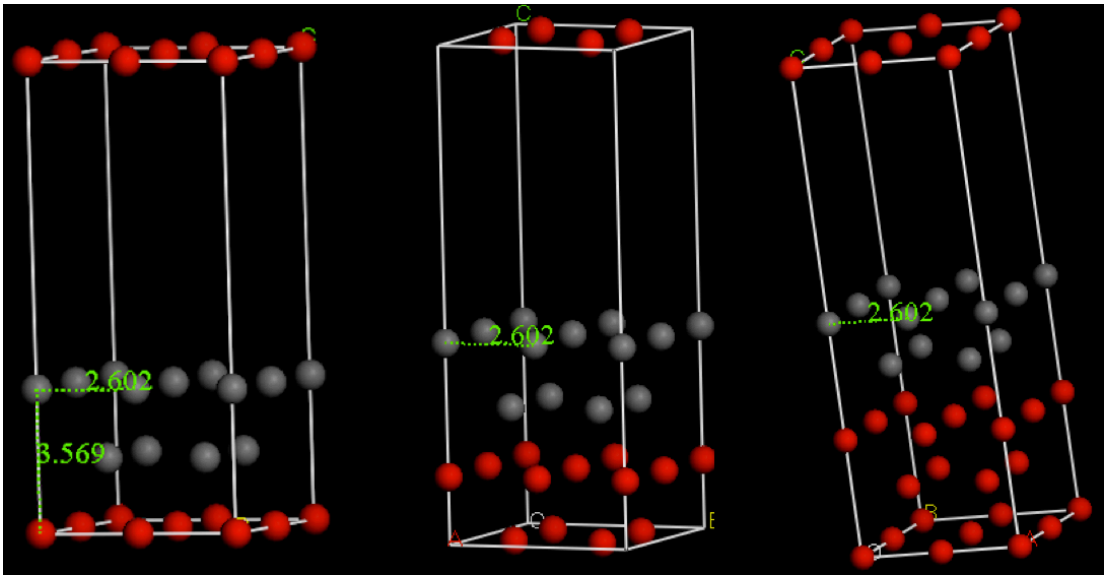

Building the Vacuum Slab

For each of the 3 facets, a vacuum slab of 10 Å thickness is built, which ensures no interactions between the surfaces at periodic boundaries.

4.5.4 Adding CO to Different Adsorption Sites

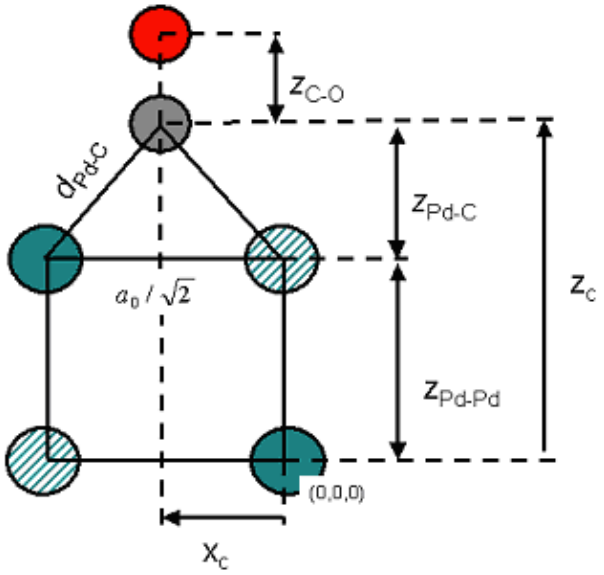

Figure 20 shows an example of how one can add the CO molecule on the short-bridge site of the Pd(110) surface. Z_{C-O} denotes the internal C-O bond length, which is put in accordance to the optimized free CO molecule in our calculations. d_{Pd-C} is the metal-CO distance; this distance is specified in our calculations from the experimental data, which is 1.90 Å. In *Figure 21-23*, a selected set of figures showing the positions of the CO molecules at different adsorption sites at different surfaces is presented.

Top-Site Adsorption

The ontop adsorption shows a slight tilting of 3 degrees from the vertical position as shown in *Figure 21*

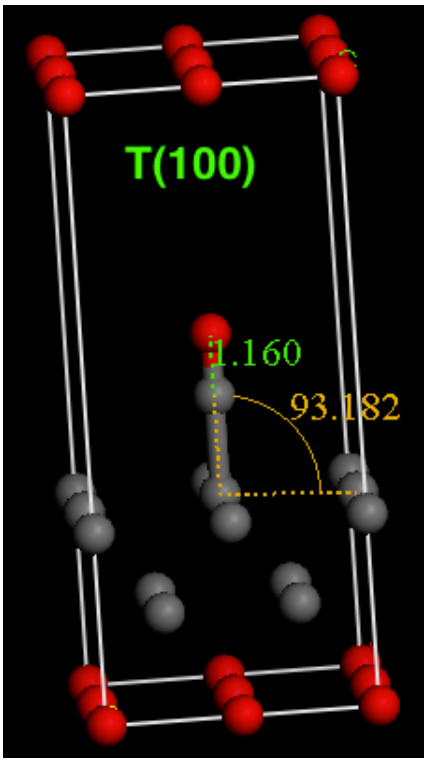

Bridge-Site Adsorptions

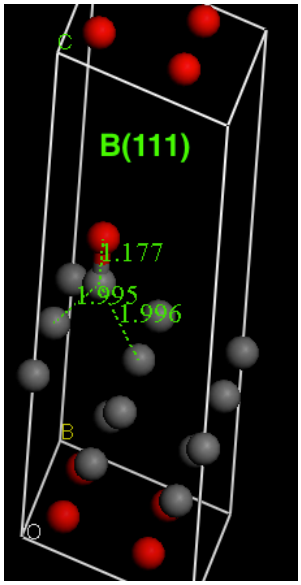

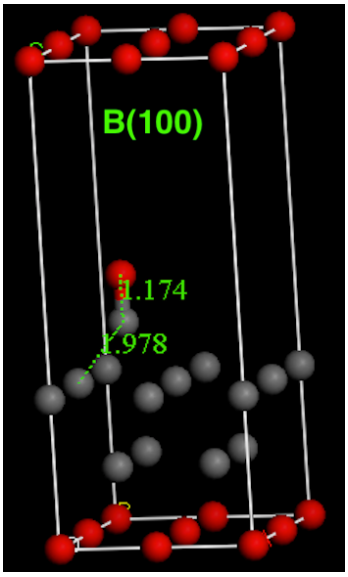

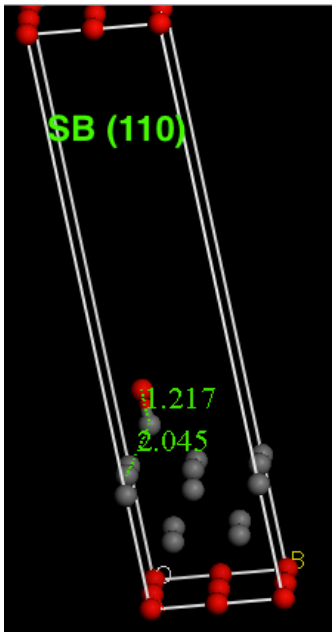

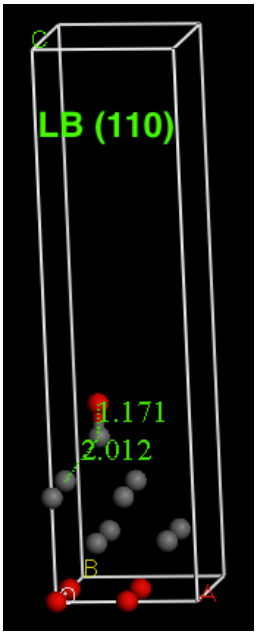

Hollow-Site Adsorptions

At the (111) surface, the difference between the fcc and hcp hollow site adsorptions is that at the fcc, there is no Cu atom beneath the adsorbed CO molecule at the second layer, whereas, for the hcp, there exist a Cu atom beneath CO molecule at the second layer.

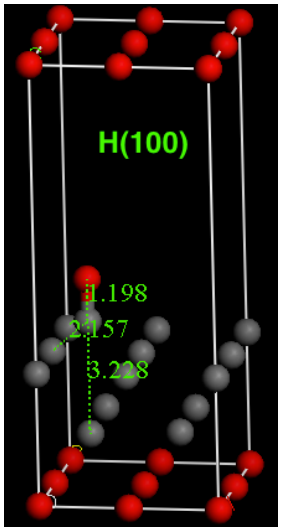

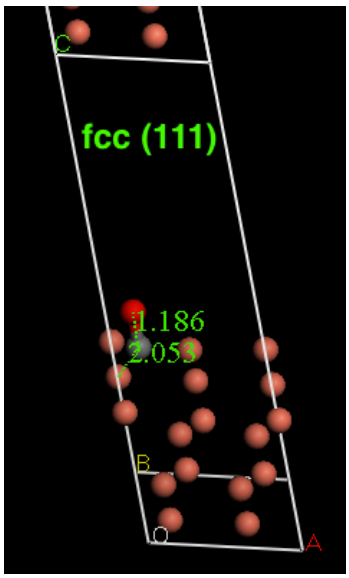

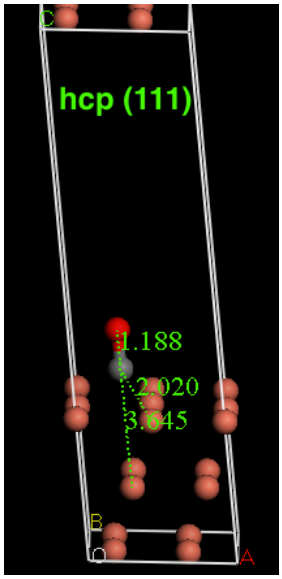

4.5.6 Calculating Adsorption Energies

Density functional theory calculations have been performed within the generalized gradient density approximation in the revised Perdew-Burke-Ernzerhof parametrization, RPBE, as modified by Hammer *et al*[4]. Calculations were done using the Cambridge Serial Total Energy Package, CASTEP, and employed ultrasoft pseudopotentials. To study the effect of adsorption on the adsorbed molecule, the electronic structure of CO is first calculated as an isolated (free) molecule and then studied after adsorption within the metal-adsorbate system. This procedure is also implemented for each of the (100), (110), and (111) surface facets. Over each surface, the chemisorption process on all the available adsorption sites – top, hollow, and bridge – are calculated. In order to exclude the CO-CO interactions that can make the electronic structure analysis more complex, the adsorption mechanism is studied for surfaces with a 1⁄4 monolayer coverage[5].

The adsorption process is modelled on a 3-layer supercell slab, separated by vacuum of 10 Å thickness, with the bottom layer atoms fixed in position and the top two layers and the CO molecule are allowed to relax. To confirm the sufficiency of the 3-layer substrate model, adsorption energies are calculated for 4-layer and 5-layer slab models, where accurate adsorption energies are found within good agreement with experimental and theoretical values reported in references[6,7]. The energy cut-off has been fixed for all surfaces at 580 eV, which is found reliable to give converged results for the systems considered. Using the Monkrokhst-Pack scheme for performing Brillion zone integrations, the k-point sampling is varied, while performing energy calculations for the isolated CO molecule, clean surfaces, and CO-substrate complexes at different surfaces. The converged

k-point samplings used for the results presented are (3x3x1) for the (100) and (111) surfaces, and (2x3x1) for the (110) surface, keeping the k-point separation fixed for all systems at 0.07 $Å^{-1}$. The effect of the deformation energy of the Cu model after CO adsorption was checked by recalculating the adsorption energies with the substrate atoms frozen in space. The deformation energy of Cu atoms is found to contribute very little change (~0.05 eV) to the adsorption energy values, insignificant to affect the site preference.

The adsorption energy is calculated by subtracting the energy of the surface-adsorbate complex from the summation of the individual clean surface and CO molecule energies before adsorption, as follows:

$$E_{Ads} = E_{complex} - (E_{surface} + E_{CO}) \qquad (4.1)$$

Since chemisorption is an exothermic reaction, the calculated adsorption energy will have a negative value, which means that when the CO molecule and the surface interact, they become more stable than they are individually.

References

1. Sholl, D. S. & Steckel, J. A. *Chapter 03: Nuts and Bolts of DFT Calculations*. *Density Functional Theory: A Practical Introduction* (2009). doi:10.1002/9780470447710.ch3
2. Sholl, D. S. *DFT Calculations for Surfaces of Solids*. *Density Functional Theory* (Wiley, 2009). doi:10.1002/9780470447710.ch4
3. Visualizer, M., Time, C. & Pd, T. Adsorption of CO onto a Pd (110) surface. **20,** 1–12 (2014).
4. Hammer, B., Hansen, L. & Nørskov, J. K. Improved AdsorptionEnergetics within Density-Functional Theory using Revised Perdew-Burke-Ernzerhof Functionals. *Phys. Rev. B* **59,** 7413–7421 (1999).
5. Mason, S. E., Grinberg, I. & Rappe, A. M. Adsorbate-adsorbate interactions and chemisorption at different coverages studied by accurate ab initio calculations: CO on transition metal surfaces. *J. Phys. Chem. B* **110,** 3816–3822 (2006).
6. Stroppa, A., Termentzidis, K., Paier, J., Kresse, G. & Hafner, J. CO adsorption on metal surfaces: a hybrid functional study with plane wave basis set. *Phys. Rev. B* **76,** 32 (2007).
7. Gajdoš, M. & Hafner, J. CO adsorption on Cu(1 1 1) and Cu(0 0 1) surfaces: Improving site preference in DFT calculations. *Surf. Sci.* **590,** 117–126 (2005).

Chapter 5

Results and Discussion

CO adsorption on both Cu and Ni (100), (110), and (111) surfaces has been extensively studied using Kohn-Sham density functional theory calculations. A holistic analysis of adsorption energies, charge transfer, and structural changes has been employed to highlight the variations in adsorption mechanisms upon changing the surface type and the adsorption site. Each surface, with its unique arrangement of atoms, resulted in a varying adsorbate behavior, although the same adsorption site is considered. This directly reflects the influence of the atomic arrangement on the substrate-adsorbate interactions. Site-interactions are rigorously investigated from molecular-orbital and charge transfer principles taking into account the fundamental interaction of frontier orbital (5σ and $2\pi^*$) orbitals. By considering the effects surface atomic arrangement and the density of metal interacting orbitals, along with the relative *d*-5σ and *d*-$2\pi^*$ energy spacings, the calculated adsorption preferences to higher coordination sites is explained, which also revealed valuable interpretations to the renown DFT CO *adsorption puzzle*. In addition, we studied the perturbations occurring upon adsorption to the 3σ and 1π orbitals, which hold the internal C-O bond. Studying 3σ and 1π orbitals perturbations provided wealth theoretical interpretations to the varying behavior of the adsorbate molecule when similar adsorption sites are compared at different facets.

* Parts of this chapter were published in the following paper: Kareem M. Gameel, Icell M. Sharafaldin, Amr U. Abourayya, Ahmed H. Biby, Nageh K. Allam, "*Unveiling CO Adsorption on Cu Surfaces: New Insights from Molecular Orbital Principles*", PCCP Journal

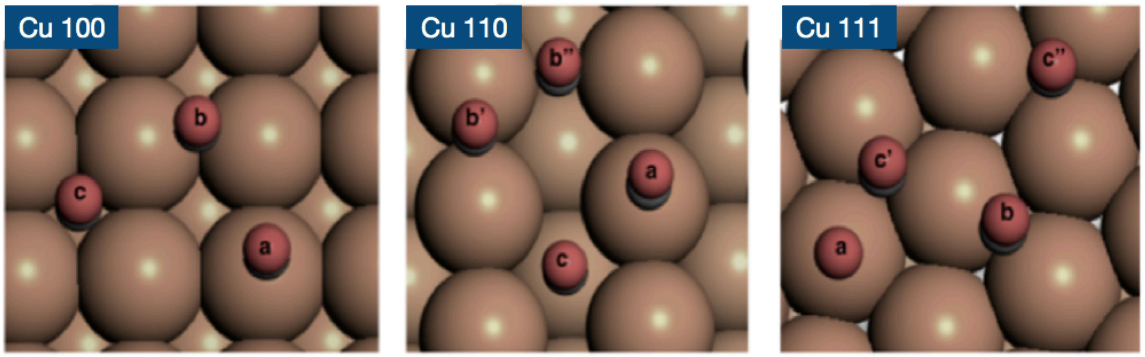

5.1 Energy Calculations

Tables 1-3 from the left to right columns, show the energy results of the free CO molecule, the clean surface, the surface-adsorbate complexes, and the calculated adsorption energies according to equation (4.6). Rows highlighted in yellow denotes the adsorption sites with the lowest adsorption energies, i.e. the preferred adsorption site.

Table 1. Cu(100) Adsorption Energies

Ads. Site	CO	Cu (100)	Cu(100)-CO	E_{ads} 100
Top	-596.0095	-20175.078	-20771.64	-0.5524
Bridge	-596.0095	-20175.078	-20771.562	-0.474
Hollow	-596.0095	-20175.078	-20771.328	-0.2399

Table 2. Cu(110) Adsorption Energies

Ads. Site	CO	Cu(110)	Cu(110)-CO	E_{ads} 110
Top	-596.0095	-20172.813	-20769.506	-0.6836
SB	-596.0095	-20172.813	-20769.676	-0.8536
LB	-596.0095	-20172.813	-20769.1	-0.2782
Hollow	-596.0095	-20172.813	-20768.886	-0.06414

Figure 24. Adsorption site
facets: (a: ontop, b: bridge

Table 3. Cu(111) Adsorption Energies

Ads. Site	CO	Cu (111)	Cu(111)-CO	E_{ads} 111
Top	-596.0095	-20175.91	-20772.199	-0.2797
Bridge	-596.0095	-20175.91	-20772.236	-0.3168
fcc	-596.0095	-20175.91	-20772.307	-0.3877
hcp	-596.0095	-20175.91	-20772.296	-0.3767

5.2 Geometrical Results

Tables 4-6 present the geometrical data. The depth is calculated as the reciprocal of the vertical height above the metal surface. The Depth column for each surface is calculated as the reciprocal of the vertical length between the carbon end of the molecule and the metal surface.

Table 4. Cu(100) Geometrical Results

Adsorption Site	C-O	M-CO	Vertical Length	Depth
Top	1.158	1.867	1.87	0.54
Bridge	1.171	2.014	1.55	0.65
Hollow	1.188	2.212	1.27	0.79

Table 5. Cu(110) Geometrical Results

Adsorption Site	C-O:	M-CO	Vertical Length	Depth
Top	1.156	1.857	1.857	0.539
Short	1.173	1.972	1.86	0.67
Long	1.178	2.082	1.34	0.744
Hollow	1.191	2.45	0.80	1.25

Table 6. Cu(111) Geometrical Results

Adsorption Site	C-O:	M-CO	Vertical Length	Depth
Top	1.159	1.856	1.85	0.54
Bridge	1.176	1.982	1.47	0.68
hcp	1.183	2.055	1.38	0.72
fcc	1.183	2.044	1.37	0.73

5.3 Charge Transfer Data

Tables 7-9 show the orbital charge transfers for Cu atoms and CO molecule.

Table 7. CO-Cu(100) Charge Transfer

Orbitals	top	bridge	hollow
CO – *s orbital*	-0.26	-0.29	-0.29
CO – *p orbital*	0.38	0.58	0.74
Total CO Gain	**0.12**	**0.29**	**0.45**
Cu – *s orbital*	-0.29	-.28	-0.32
Cu - *p orbital*	0.33	0.16	0.10
Cu - *d orbital*	-0.15	-0.18	-0.22
Total Cu Loss	**-0.11**	**-0.30**	**-0.44**

Table 8. CO-Cu(110) Charge Transfer

Orbitals	top	Short-bridge	Long-bridge	Hollow
CO – *s orbital*	-0.24	-0.28	-0.29	-0.31
CO – *p orbital*	0.35	0.57	0.64	0.74
Total CO Gain	**0.11**	**0.29**	**0.35**	**0.43**
Cu – *s orbital*	-0.14	-0.16	-0.22	-0.36
Cu - *p orbital*	0.12	0.04	-0.02	0.06
Cu - *d orbital*	-0.09	-0.18	-0.11	-0.14
Total Cu Loss	**-0.11**	**-0.30**	**-0.34**	**-0.43**

Table 9. CO-Cu(111) Charge Transfer

Orbitals	top	bridge	hcp	fcc
CO – *s orbital*	-0.28	-0.31	-0.32	-0.30
CO – *p orbital*	0.39	0.62	0.69	0.68
Total CO Gain	**0.11**	**0.31**	**0.37**	**0.38**
Cu – *s orbital*	-0.23	-0.29	-0.33	-0.32
Cu - *p orbital*	0.21	0.11	0.07	0.09
Cu - *d orbital*	-0.09	-0.12	-0.11	-0.14
Total Cu Loss	**-0.11**	**-0.30**	**-0.37**	**-0.37**

5.4 Validating the Accuracy of Results

From the results presented in Table 10, we can see that the calculated C-O and Cu-C bond lengths in a very good agreement with experimental value. The calculated adsorption energies of CO are in reasonable agreement with the experimental adsorption energies; on Cu(111) surface, the adsorption energy is underestimated by ~0.14 eV compared to the experimental values, whereas adsorption energies at the Cu(100) are found in good agreement with the experimental values.

According to the Blyholder model[1], the surface bonding is depicted through a two-step interaction process initiated by a 5σ charge donation followed by a 2π* back donation. As the adsorption coordination number increases so does the overlap between the metal states and the LUMO 2π* orbitals. Since the 2π* is an anti-bonding orbital, any charge added through back- donation results in a C-O internal bond stretching, implying a more dissociative fashion. The results in *Figure 25* shows a linear correlation between the charge transfer from the metal surface to the CO molecule and the stretching of the C-O bond-

Table 10. Structural and Energy Results, adsorption energy, Cu-C bond lengths (d_{Cu-C}), and C-O bond lengths (d_{C-O}) results are displayed. At a coverage of Θ= ¼ ML, theoretical and experimental data from literature are compared with our calculated results. The theoretical data from literature are selected from ref.[6], where RPBE functional is utilized with projected augmented plane waves at 450 eV energy cutoff. The experimental data are put in square brackets; bond lengths are on average within an accuracy of 0.1 Å. The numbers put in **bold** correspond to the preferred adsorption sites.

		Literature			***Calculations***		
Surface	***Site***	***Adsorption energy (eV)***	***d_{C-O} (Å)***	***d_{Cu-C} (Å)***	***Adsorption energy (eV)***	***d_{C-O} (Å)***	***d_{Cu-C} (Å)***
Cu(100)	***Top***	**-0.565 [-0.53, -0.57]** Ref.[7,8]	**1.162 [1.13, 1.15]** Ref.[9]	**1.87 [1.90, 1.92]** Ref.[9,10]	**-0.5524**	**1.158**	**1.867**
	Bridge	-0.545	1.176	2.01	-0.474	1.171	2.014
	Hollow	-0.471	1.200	2.18	-0.2399	1.188	2.212
Cu(110)	***Top***	**[-0.63]** Ref.[7]	**[1.11]** Ref.[11]	**[1.87]** Ref.[11].	-0.6836	1.156	1.857
	Bridge	-	-	-	**-0.8536**	**1.173**	**1.972**
	Long-bridge	-	-	-	-0.2782	1.178	2.082
	Hollow	-	-	-	-0.06414	1.191	2.45
Cu(111)	***Top***	**-0.42 [-0.43, -0.52]** Ref.[7,12,13]	**1.162**	**1.187 [1.91]** Ref.[14]	-0.2797	1.159	1.856
	Bridge	0.39	1.179	2.01	-0.3168	1.176	1.982
	hcp	-0.45	1.185	2.08	-0.3767	1.183	2.055
	fcc	-0.46	1.185	2.08	**-0.3877**	**1.183**	**2.044**

length, as the coordination number increases. The change in depth of adsorption and the Metal-C bond length also verify a direct relation with charge back-donation, which is attributed to the degree of overlap between metal orbitals and the CO 2π* antibonding orbitals. The results of the calculated Mulliken population support this claim, indicating an increase in the charge gained by the CO-p orbitals, which forms the 2π*, as the coordination number increases. On the contrary, the data of the adsorption energies (Eads), *Figure 25a*, indicates no correlation with the coordination number or charge transfer, when different

surface types are compared. These results imply that the adsorption energetics cannot be used as a descriptor for the bonding mechanism, but rather as a solo descriptor for the site preference and stability of the adsorption reaction. The results of Föhlisch *et al*[2] confirm this conclusion, where the C-O stretch frequency shift differed only marginally upon adsorption on Cu and Ni surfaces, whereas the adsorption energy had doubled. Thus, they showed that the C-O bond strength is not related to the adsorption energy and that no conclusions about the bonding mechanism can be drawn from the Eads results.

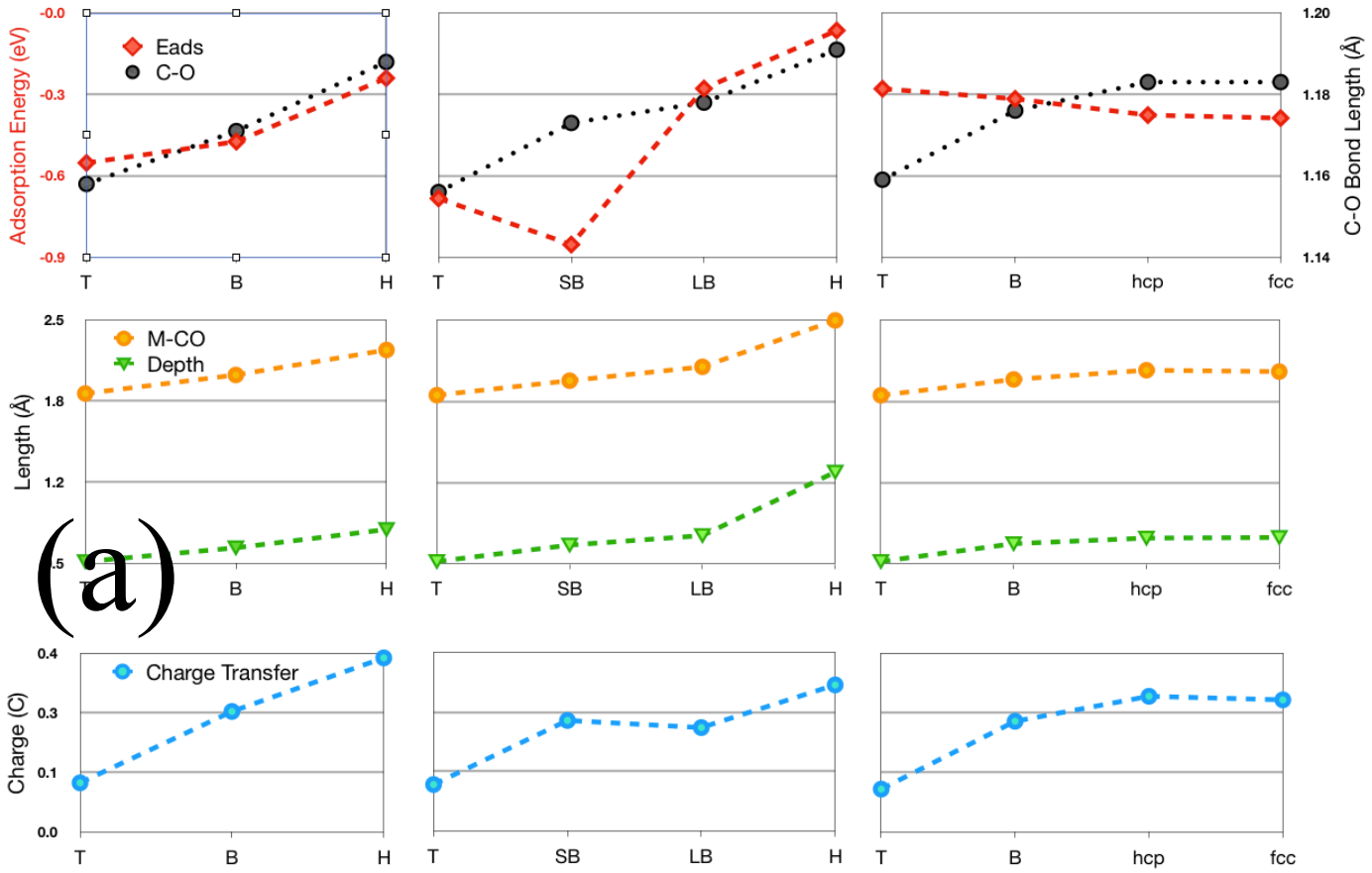

In order to grasp a detailed chemisorption picture based on DFT electronic structure investigations, it is necessary to understand how DFT inaccurate prediction of electronic structures directly influences the chemisorption thermodynamics, which in turn leads to contradicting site preference estimations. By doing so, we can verify that the accuracy of electronic structure picture will only affect the site preference without affecting the local bond-characteristics that is unique for each adsorption site.

5.5.1 Interpreting the CO Adsorption Puzzle

Previous experimental measurements have indicated that, at low surface coverage, the CO molecule prefers on-top adsorption site for all Cu surface facets. However, our DFT calculations predict an on-top site preference for the Cu(100) surface only, while predicting short- bridge and hollow (fcc) site preferences for the Cu(110) and Cu(111) surfaces, respectively. The reason behind the contradicting results can be directly attributed to the inaccurate electronic structure predicted by the semilocal density functional calculations.

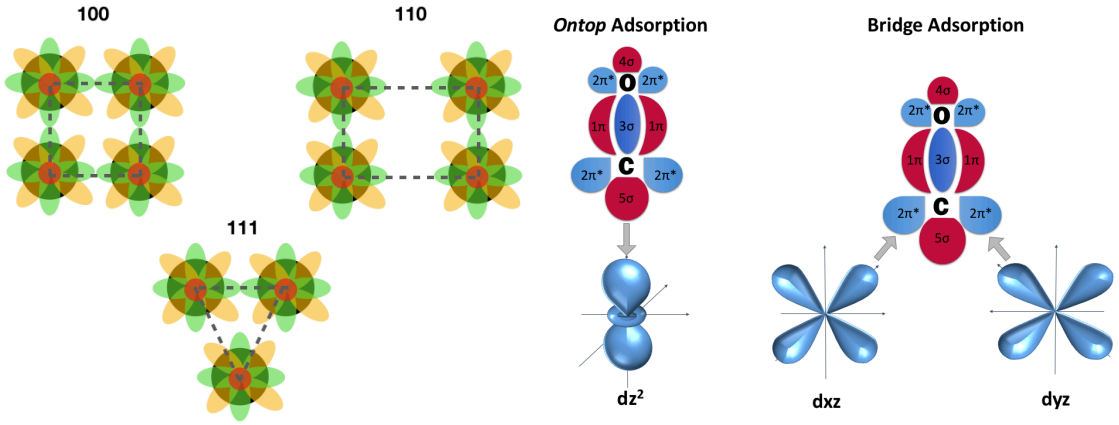

However, even with the use of more accurate hybrid Hartree-Fock density functionals calculations, correct site preferences are only obtained for closed d-shell orbitals and fail to predict correct site preferences for other transition metals, especially at the (111) surface. For this reason, other bonding parameters must be considered along with the electronic properties to decipher the CO adsorption puzzle.

Comparing HSE03 calculation results, done by Stroppa *et al*[27], with our semilocal RPBE density functional calculation results, we can observe discrepancies in the predicted CO 5σ-2π* gap and their relative positioning with respect the Cu *d*-band center for the Cu(111) surface. As shown in *Figure 27*, the 2π* orbital is downshifted closer to the *d*-center and the 5σ-*d*-center gap is extended. Thus, RPBE calculations make the 2π*-*d*-orbital overlap more favorable, and contrariwise, make the 5σ-*d*- orbital interaction less favorable, compared to the HSE03 calculations. For each surface facet, orbitals energy calculations show that the *d*-center positioning relative to the 5σ and 2π* orbitals to be changing according to the surface type, as shown in *Figure 27*. From the same figure, we can find that the (110) surface has the widest 5σ-*d* gap, while having the narrowest 2π*-*d* gap, compared to the other surfaces. Although the 2π*-*d* energy gap is still larger than that of the 5σ-*d* gap, the spatial proximity between the CO 2π* and the *dxz/dyz* orbitals of the nearest two neighboring Cu atoms (Figure 26) makes the 2π*-*d* overlap more favorable. At the short-bridge, the CO molecule can adsorb deeper getting closer the metal *d*-orbitals. Therefore, the factor of energy proximity due 2π*-orbital, due energy shifting closer to the *d*-center, added to the factor of spatial proximity between 2π*-*dxz/dyz* orbitals at the short-

bridge site, make the $2\pi^*$-*dxz/dyz* more significant than the 5σ- d_z2 interaction and results in the short-bridge site preference at the (110). At the (100) surface, the most stable adsorption site is found to be the top site, despite the fact that the orbital concentration at the (100) bridge site is equal to that of the (110) short-bridge site. This inconsistency is attributed to the relative orbitals' energy positioning (***Figure 27***); the 5σ-*d* gap is noticeably shorter at the (100) surface compared to the (110) surface. Therefore, at the (100), the spatial factor of higher *d*- orbital density at the bridge-site is not sufficient for the $2\pi^*$-$d_{XZ/YZ}$ interaction to surpass the 5σ-d_Z2 orbital overlap at the top site, leading to a top-site preference.

For the (111) surface, *Figure 24a* elaborates a higher orbital density at the bridge and hollow sites, compared to the other surfaces. This makes the metallic *d*-orbitals spatially closer to the CO $2\pi^*$ orbitals. Thus, the narrowing of the $2\pi^*$-*d* energy gap makes

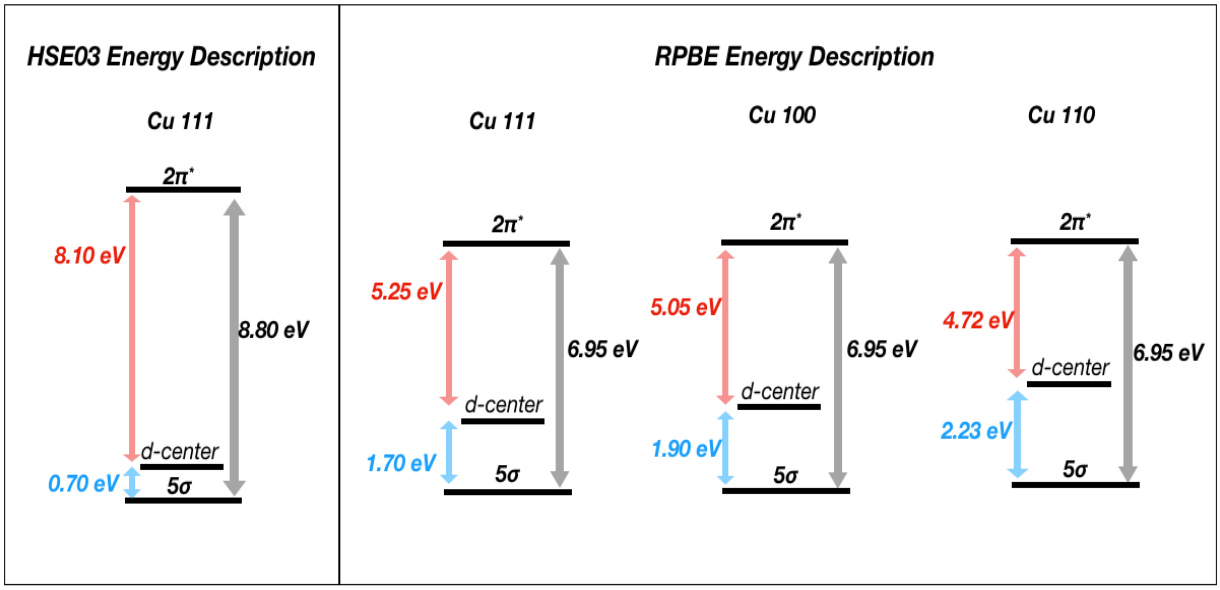

the higher coordination sites more favorable for adsorption, which is confirmed in *Figure 25*a. Consequently, the compressed atomic stacking of the (111) surface reflects the reason behind stubborn favor of higher coordination sites by DFT calculations, even when more expensive calculations are employed. Since the highest concentration of *dxz/dyz* orbitals is found at the hollow-site when compared to the top and bridge sites (Figure 26a), a more significant $2\pi^*$-*dxz/dyz* orbitals interaction can be claimed, favoring the hollow (fcc) site preference; nearly degenerate with the hollow (hcp) site.

Since it is now proved that site-preference predictions are merely dependent on both the orbitals' spatial and energy levels positionings, the contradicting site preferences do not necessarily imply inaccurate predictions of local bond properties. This is also proven by the absence of correlation between the adsorption energy and the structural and charge transport trends, elaborated in *Figure 25*. Therefore, we can reliably utilize DFT calculations to investigate complex bonding mechanisms from molecular orbital and charge transport principles, which brings more detailed insights on the bonding mechanism.

5.5.2 Molecular Orbital and Charge Transport Insights

A molecular-orbital bonding description can be drawn by analyzing the electronic structure perturbations and tracking the charge transport occurring upon adsorption. By doing so, we can interpret the data of charge transfer and structural changes presented in *Figure 25* and get more detailed picture of electron transfer and orbital interactions within

the adsorbate- substrate complex atoms. The CO molecule is adsorbed on the surface towards the C end. Although oxygen is more electronegative, this adsorption orientation is energetically favored because of the dative O-covalent bonding within the C- O triple bond, forming a net dipole moment pointing towards the C end with larger magnitudes of the 5σ and $2\pi^*$ orbitals [96]. Upon increasing the coordination number, a general trend of increasing adsorption depths, C-O internal bond, and metal-CO bond lengths is depicted within each surface type, see *Figure 25*. The density of states (DOS) results of the adsorbate-substrate complex verifies a key contribution of the metallic *d*-states to the adsorption process, where the changes of the *d*-orbitals peaks are observed in all adsorption sites for all surfaces, manifested significantly at the *on-top* adsorption. Nonetheless, charge transfer data confirm an extensive contribution of metal *sp*-states in the bonding process. As the Cu *d*-states are fully occupied, the next energetically empty orbitals are the 4*p* states. Our population results show a substantial change in Cu *sp*-orbitals population as the coordination number increases, implying that the *p*-orbitals play a key role in the receiving charge from the CO 5σ orbital, followed by charge back- donation through the *d*-$2\pi^*$ orbital overlap. This metallic *sp*- orbital charge transfer role is not significant when partially full *d*-transition metals are concerned. For example, in ref[15], Ni surface was studied as a substrate and the metal contribution was found to be mainly through the partially full *d*-states. Thus, for Cu with fully occupied *d*-orbitals, the contribution of the empty 4*p* states become more significant.

Exploring the adsorption mechanism for *on-top* adsorption over different facets, we can spot variations in the adsorbate final structure. In order to understand these varying

behaviors, we need to look beyond the frontier orbitals and investigate the non-frontier orbitals behavior. In principle, the stronger and shorter the adsorbate-substrate bonding is, the weaker and longer the internal C-O bonding gets. The internal C-O triple bond is carried by one 3σ orbital and two 1π orbitals. On all surface facets, the 3σ shifts to higher energies as the adsorption coordination number increases, i.e. 3σ becoming less stable, as shown in *Figure 28a, c,* and *e*. Since the 3σ is a bonding orbital, as the coordination number increases, the C-O internal bond becomes less stable, and the C-O bond length stretches (*Figure 25a*). Nonetheless, for the same coordination number (at the same adsorption sites), the behavior of the 3σ and 1π orbital is different on different surface facets. For example, when the *on- top* site adsorption is compared on the different facets, as shown in *Figure 28a*, the shift of the 3σ orbital shows an inconsistent behavior over different surfaces. An extra feature, exclusive for the 1π, takes place differently at different adsorption sites, which is the broadening of the 1π peak. This broadening implies a splitting of the degeneracy of the two 1π orbitals, which reflects a less stable C-O bonding. We can now study each adsorption site at each surface one at a time, by analyzing the corresponding 3σ and 1π orbitals as follows:

On-top adsorption for different facets:

- *At the Cu(110) Top*, both the 3σ and 1π orbitals shifted to lower energies (*Figure 28a* and *b*), implying a more stable C-O internal bond. This is confirmed by the elaborated shortest *ontop* C-O bond-length at the (110), as shown in *Figure 25a*.

- *At the Cu(111) Top,* both the 3σ and 1π orbitals shifted to higher energies (*Figure 28.a* and *b*), implying a less stable C-O internal bond. This is confirmed by the elaborated longest Top C-O bond-length at the (111), as shown in *Figure 25a*.
- *At the Cu(100) Top*, the 3σ nearly stayed in the same position and 1π orbitals shifted to lower energies (*Figure 28a* and *b*), also implying a stable C-O internal bond; slightly less stable than that of the (110). This is confirmed by the elaborated intermediate Top C-O bond-length at the (100), as shown in *Figure 25a*.

Bridge adsorption for different facets:

- Comparing the bridge sites at each surface, we can spot that the 3σ shifting to a higher (less stable) energy level at the (110) compared to the (100), confirming a stronger $2\pi^*$-*d* interaction at the bridge-site of the (110) that results in a weaker C-O internal bond. The same behavior is adopted by the 1π shift at the (100) and (110), as depicted in *Figure 28c* and *d*. This overestimated $2\pi^*$-*d* interaction at the bridge-site of the (110) reflects why the short-bridge site is more favored at the (110) than the (100) surface, which resulted in a short-bridge site preference prediction that contradicts experimental *ontop* preferences.

- The long-bridge at the (110) is uniquely studied and not to be compared with the previous bridge site adsorptions. The long-bridge adsorption shows an overlapping upshift of the 3σ with that of the (111) and the largest upshift of the 1π orbital,

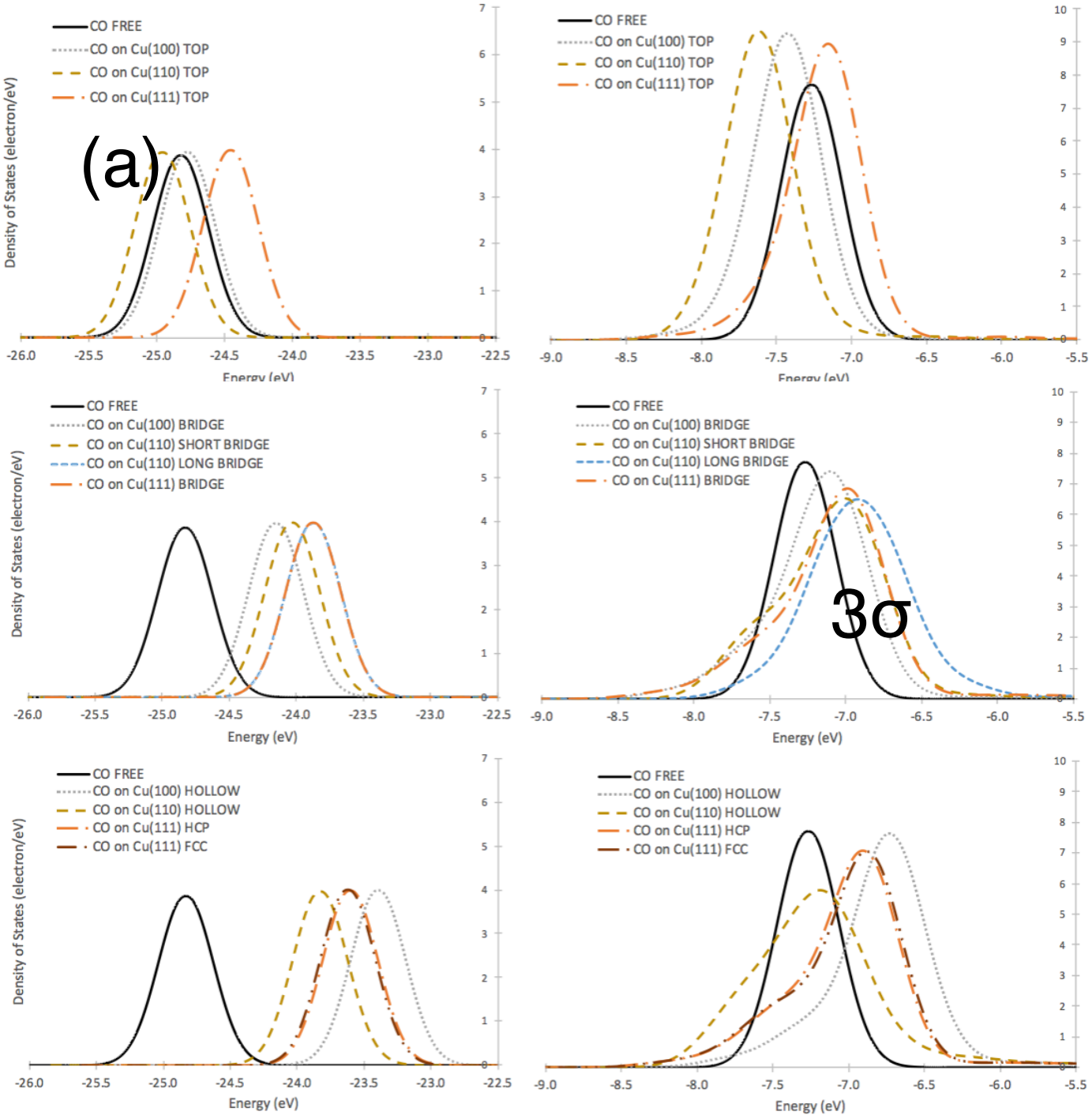
CO FREE
CO on Cu(100) TOP
CO on Cu(110) TOP
CO on Cu(111) TOP
(a)
Density of States (electron/eV)
Energy (eV)
CO FREE
CO on Cu(100) TOP
CO on Cu(110) TOP
CO on Cu(111) TOP
Energy (eV)
CO FREE
CO on Cu(100) BRIDGE
CO on Cu(110) SHORT BRIDGE
CO on Cu(110) LONG BRIDGE
CO on Cu(111) BRIDGE
Density of States (electron/eV)
Energy (eV)
CO FREE
CO on Cu(100) BRIDGE
CO on Cu(110) SHORT BRIDGE
CO on Cu(110) LONG BRIDGE
CO on Cu(111) BRIDGE
3σ
Energy (eV)
CO FREE
CO on Cu(100) HOLLOW
CO on Cu(110) HOLLOW
CO on Cu(111) HCP
CO on Cu(111) FCC
Density of States (electron/eV)
Energy (eV)
CO FREE
CO on Cu(100) HOLLOW
CO on Cu(110) HOLLOW
CO on Cu(111) HCP
CO on Cu(111) FCC
Energy (eV)

length, as shown in *Figure 25a*. This can be attributed to the large depth of the adsorbed CO molecule at the long-bridge, which makes it more prone to the $2\pi^*$-*d* orbital-field interactions that destabilizes the 1π orbitals degeneracy. The destabilization of 1π orbitals degeneracy can be depicted by the broadening of the 1π peak, as shown in *Figure 28d*. Although the largest instability of the C-O bond is witnessed at the long-bridge site, this site interaction is not thermodynamically favored due to the considerably large distance between the C and substrate atoms, compared to the other bridge sites, as depicted in the large metal-CO bond length in *Figure 25a*. This reflects the significance of spatial proximity between interacting entities on their interaction thermodynamics.

Hollow adsorption for different facets:

- At the (111), both hcp and fcc shows exact upshifts of the 3σ and 1π, as shown in *Figure 28e* and *f*. This total upshift is larger than that of the bridge-site, which reflects a stronger $2\pi^*$-*d* interaction at the hollow site that results in a nearly degenerate fcc-hcp hollow site preference.
- At the (100), the largest upshifts of the 3σ and 1π is displayed, without a significant broadening of the 1π peak. However, for the (110) hollow, the 1π orbital displayed the widest broadening, elaborated by the considerable reduction of the amplitude of the (110) 1π peak, compared to the other surfaces 1π peak amplitudes (*Figure 28* f). This significant broadening, although not shifted to higher energies, resulted in a less stable C-O bonding. From the C-O bond-lengths results at the different

hollow sites in *Figure 25a*, the longest C-O bond is found at the (110), which denotes that the effect of the 1π splitting has a more significant impact of the internal bond destabilization than the mere energy upshifts.

5.6 CO Adsorption on Cu vs. Ni Surfaces

At low coverages, the CO molecule prefers to adsorb on different sites at different Ni facets: on-top on the (100), bridge on the (110), and hollow on the (111). Our calculation predictions agree with the experimental results, except for the (100), where the hollow adsorption site is found to be the thermodynamically preferred site instead of the on-top, as shown in *Figure 29c*. Low coverage adsorption of CO on Cu is thermodynamically observed to occur at the on-top sites at all Cu facets. However, our DFT calculations predicts on-top site preference at the Cu(100) facet only, while predicting bridge- and hollow-site preferences at the Cu(110) and Cu(111) respectively. The charge transfer and structural predictions have a matching behavior that agrees with the Blyholder model bonding model, where at higher coordination sites the charge transferred from the metal to the CO molecule increases accompanied by internal C-O bond stretching, implying an increased charge population of the anti-bonding 2π* orbitals. Nonetheless, the bond stretching can additionally be attributed to the changes occurring to the 3σ and 1π bonding orbitals that hold the internal C-O bond. In reference[5], the 1π orbitals becomes depleted from electrons upon adsorption, in addition, our previous study on Cu surfaces revealed significant 3σ and 1π destabilization upon adsorption, which varied at different adsorption-sites, and were also observed to be varied according to the surface type even when the same

adsorption-site is compared. Thermodynamically, the change in adsorption energy with respect to the coordination number at different surfaces reveals no defined correlation between coordination number and adsorption energy. Therefore, from the adsorption energy results, we can determine the most stable adsorption site, however, we cannot utilize them to describe the local bond properties. To confirm this notion, the C-O bond length at the on-top adsorption on the Ni(100) is equal to that at the Ni(110), however, the adsorption

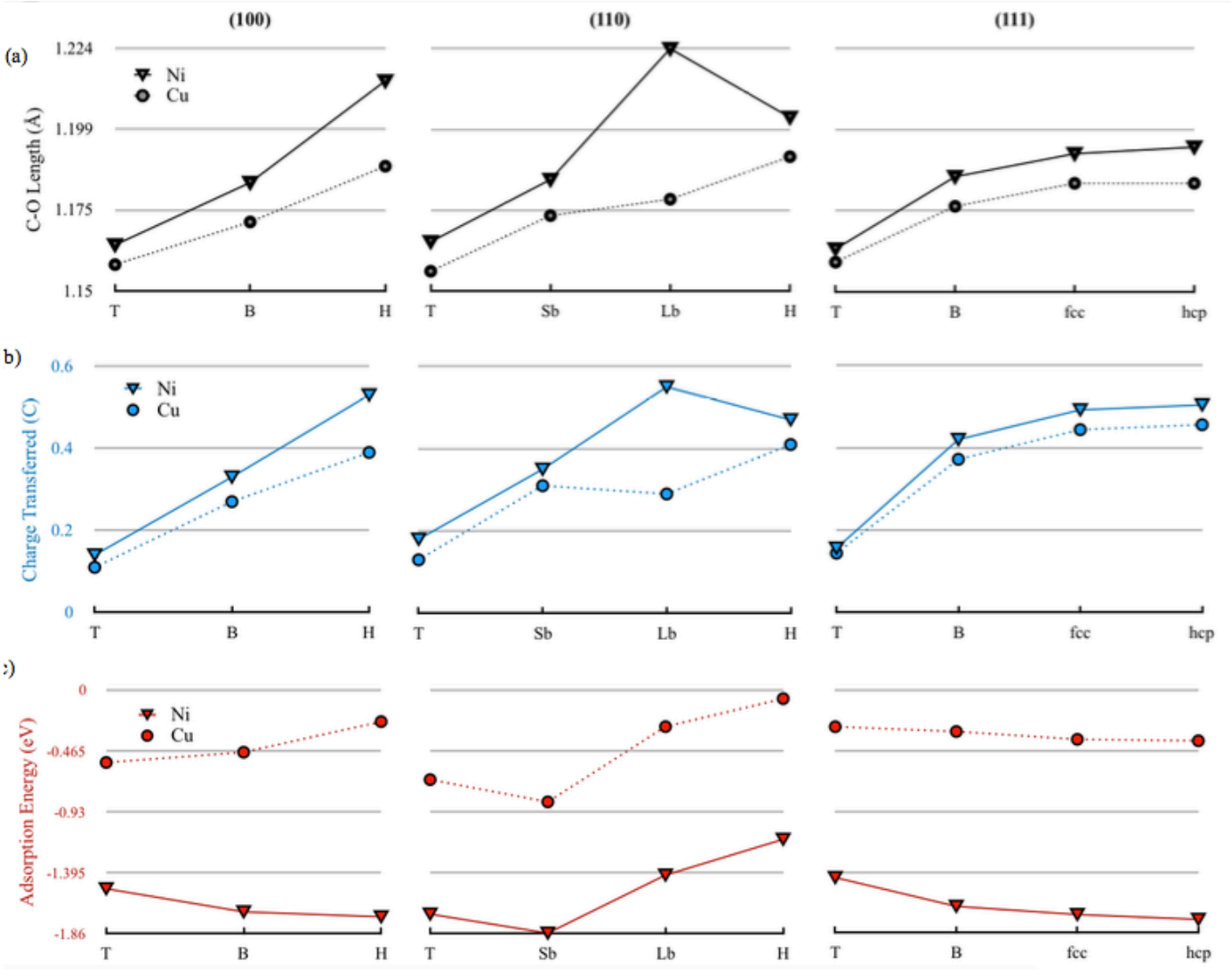

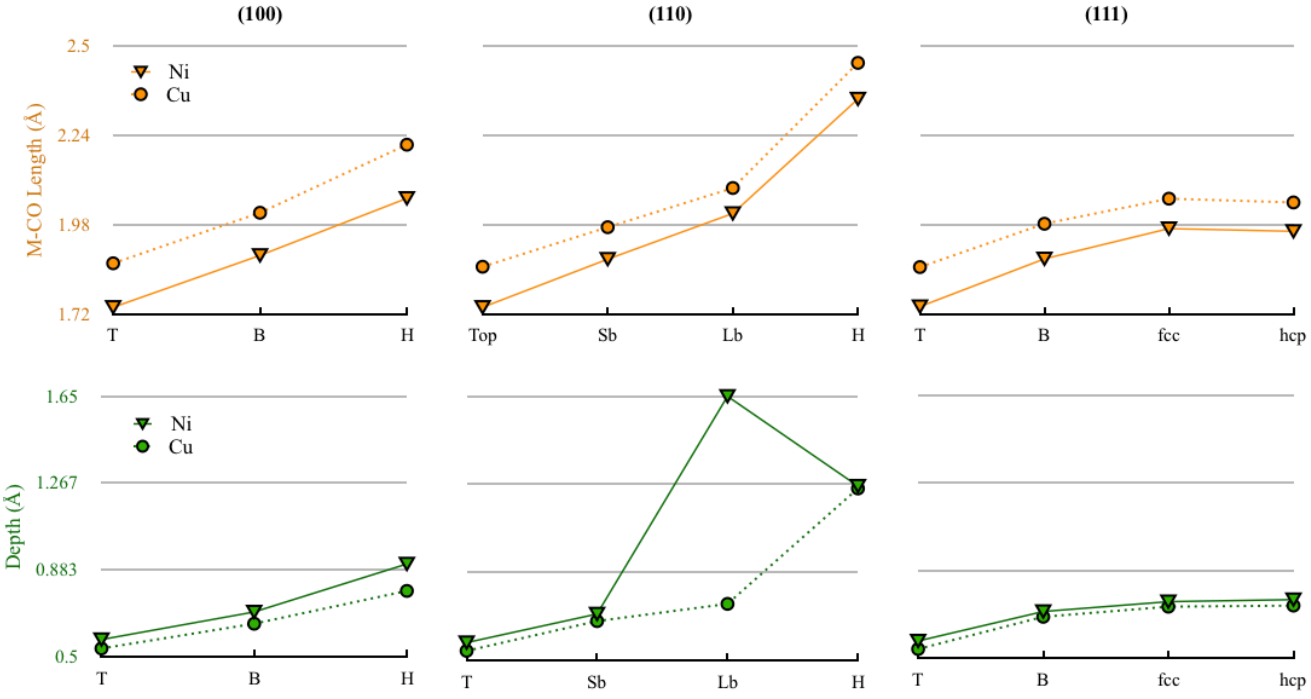

at the Ni(110) is more stable by 0.2 eV , implying that the internal C-O bond strength is not related to the adsorption energy results.

5.6.1 Angular Momentum Contributions in Charge transfer

The tables in this section presents the charge transfer results in the metal s, p, and d orbitals. In the column in the middle (sp), the total charge gain/loss in the sp states is presented. The column at the far right, represents the net charge gain/loss at the metal surface. These results can give us insights on the true nature of the σ-interaction.

Cu Charge Transfers

Table 11. Cu(100) Atomic Orbitals Charge Distribution

Cu100	***s***	***p***	***sp***	***d***	***net***
top	-0.29	0.33	0.04	-0.15	-0.11
bridge	-0.28	0.16	-0.12	-0.18	-0.3
hollow	-0.32	0.10	-0.22	-0.22	-0.44

Table 12. Cu(110) Atomic Orbitals Charge Distribution

Cu110	***s***	***p***	***sp***	***d***	***net***
top	-0.14	0.12	-0.02	-0.09	-0.11
sb	-0.16	0.04	-0.12	-0.18	-0.3
Lb	-0.22	-0.02	-0.24	-0.11	-0.35
hollow	-0.36	0.06	-0.3	-0.14	-0.44

Table 13. Cu(100) Atomic Orbitals Charge Distribution

Cu111	***s***	***p***	***sp***	***d***	***net***
top	-0.23	0.21	-0.02	-0.09	-0.11
b	-0.29	0.11	-0.18	-0.12	-0.3
hcp	-0.33	0.07	-0.26	-0.11	-0.37
fcc	-0.32	0.09	-0.23	-0.14	-0.37

Ni Charge Transfers

Table 14. Ni(100) Atomic Orbitals Charge Distribution

Ni100	**s**	**p**	**sp**	**d**	**net**
top	-0.22	-0.02	-0.24	0.07	-0.17

bridge	-0.3	-0.21	-0.51	0.14	-0.37
hollow	-0.39	-0.3	-0.69	0.14	-0.55

Table 15. Ni(110) Atomic Orbitals Charge Distribution

Ni110	**s**	**p**	**sp**	**d**	**net**
top	-0.11	-0.05	-0.16	-0.09	-0.25
sb	-0.18	-0.18	-0.36	-0.18	-0.54
Lb	-0.42	-0.2	-0.62	-0.11	-0.73
hollow	-0.39	-0.13	-0.52	-0.14	-0.66

Table 16. Cu(111) Atomic Orbitals Charge Distribution

Ni 111	**s**	**p**	**sp**	**d**	**net**
top	-0.16	0.06	-0.1	-0.09	-0.19
b	-0.25	-0.08	-0.33	-0.12	-0.45
hcp	-0.28	-0.14	-0.42	-0.11	-0.53
fcc	-0.27	-0.12	-0.39	-0.14	-0.53

5.7 The Blyholder-Nilsson & Peterson (BNP) Model

Since its formulation in the 1964, Several later models and refinements have been proposed, with most of them in agreement with the original Blyholder model. Some of the models that are conforming under the name “Blyholder Model” are principally in disagreement with the original Blyholder model. In these models, only the frontier (5σ and 2π*) orbitals of the CO molecule are modified during the chemisorption process through a simple 5σ donation to the substrate atoms followed by a 2π* backdonation, whereas the

original Blyholder rather proposes a hybridization of the CO π-orbitals with the metallic d-orbitals to form a dπ band. Nonetheless, the reason why the simple, yet inaccurate, frontier orbital model adopted was commonly accepted and adopted in literature as it was validated for a number of reasons. First, because of the observed population of charge at the 2π* orbitals that increases with the increase of the coordination number. Also, due to the shift of 5σ orbital to higher binding energies upon adsorption, which was interpreted as a sign of attractive 5σ donation. Furthermore, results from theory indicate that adsorption energetics can be described in terms of the positions of the 2π* and the metal d-band center only. All these findings supported the simple 5σ donation and 2π* backdonation model, where the other orbitals are not affected by the interaction.

Within the BNP, the energetics of adsorption is depicted as the result of the synergism between σ-repulsion and π-attraction, where both of the two interactions increase with the increase in the substrate coordination number. Therefore, at any surface, the adsorption site on-which the π-attraction surpasses the σ-repulsion the most will be the most energetically favored site for adsorption. Nonetheless, the character of σ-interaction as attractive or repulsive is still a controversial issue, whereas the attractive nature of π-interaction is generally accepted.

For the σ-interaction being considered to be having an entirely repulsive nature within the BNP model, the CO preference of on-top adsorption at all surfaces, was interpreted due to the increased σ-repulsion at higher Cu coordination that exceeds the increase in π-attraction, leading to the preference of low Cu coordination sites. At longer molecule-metal bond distances the Pauli repulsion becomes smaller, and since the Cu-CO bond distances are larger than that of Ni (see *Figure 30*c), σ-repulsion in Cu is expected to

be smaller. In addition, although Cu has a nearly closed d-orbital occupancy compared to a $d^{8.4}$ occupancy in Ni, charge population of the empty Cu 4p-orbitals is detected upon adsorption, which can be inferred as a bonding 5σ donation to the empty Cu p-orbitals. Based on the Cu 4p charge gain, we can now assume that the σ-interaction in Cu is both partially repulsive and partially attractive, with a more dominant repulsive nature. Repulsive in the sense of Pauli-repulsion between 5σ and the d-orbitals, and attractive via the charge donation from the 5σ to the *sp*-states of the Cu atoms. The p-gain is also observed to be decreasing at higher Cu coordination, implying that the 5σ partial attraction decreases at higher Cu coordination, which implies a larger 5σ interaction dominancy at lower coordination sites. The larger 5σ partial attraction at lower Cu coordination can interpret the on-top site preference that is experimentally found at all Cu surfaces, where the 5σ interaction with metallic p_z becomes more pronounced, due to matching symmetry. On the other hand, the p-states of Ni is found to be depopulated of charge upon adsorption, in contrary to what happens in Cu, see tables 11-16. Also, the Ni 3p charge depopulation is found to be increasing at higher Ni coordination. The Ni p-orbitals depopulation can be interpreted as a sign of a repulsive σ-interaction, where orbitals are depleted from charge to minimize the repulsion as much as possible, and can also be interpreted as a sign of a stronger π-bonding interaction, where charges are spread across the dπ band.

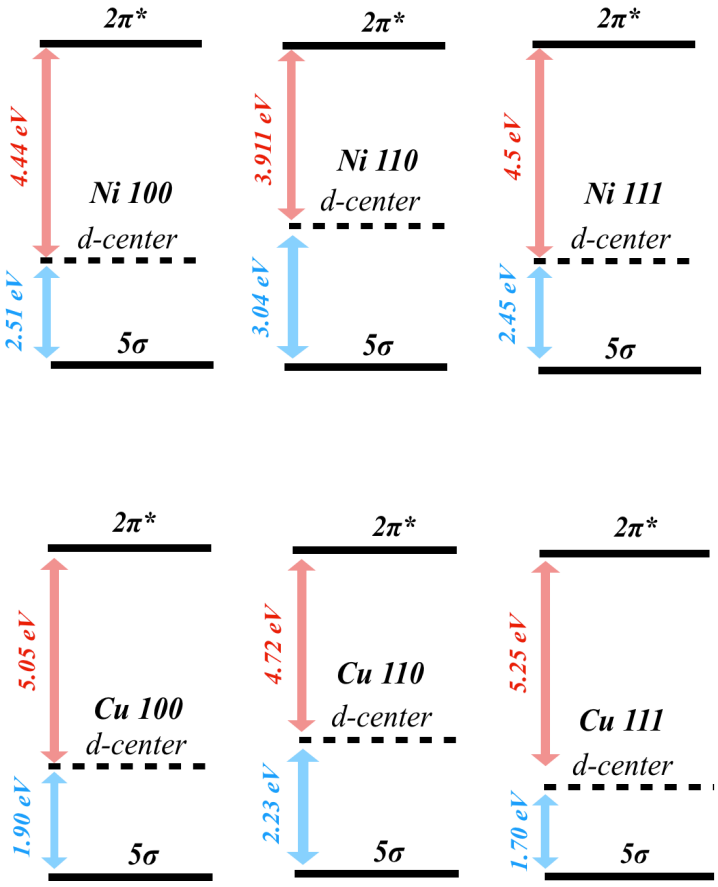

Energetically, when we compare the orbital energy positions in Ni and in Cu, see *Figure 31*, we can observe that d-2π* gap is on average shorter by 0.72 eV in Ni, leading to a generally enhanced π-interaction in Ni. The enhanced π interactions in Ni is reflected in the larger C-O bond lengths when compared with Cu, as seen in *Figure 29*. More significantly, the 5σ orbital energy is further away from d-center in Ni by an average of 2.17 eV than in Cu, leading to a significantly weaker 5σ-d interaction in Ni than in Cu. The proximity between the CO 5σ and the Cu d-center makes the σ-interaction stronger, with a stronger partial σ-attraction at lower Cu coordination. Whereas the proximity between the

$2\pi^*$ and the Ni d-center implies a stronger π-interaction that is enhanced at higher Ni-coordination.

5.7.1 Interpreting the CO Adsorption on Ni using the BNP Model

Comparing the CO adsorption on Ni(100) and Ni(110), we can see that, at the Ni(100), the 5σ-*d* gap is narrower by ~0.5 eV and that the *d*-$2\pi^*$ gap is wider by the same value. Thus, compared to the Ni(110), the π- attraction is weaker and the σ-repulsion is stronger, leading to generally less thermodynamically favored adsorption on the Ni(100) compared to the Ni(110). The stronger π-interaction at the Ni(110) can be validated by the more stabilized adsorption energies at the Ni(110) compared to the Ni(100). Since, the σ interaction in Ni is depicted to be fully repulsive with no partial attraction, the CO would favor to adsorb on a site where the π-interaction is strong enough to give the largest net attraction. Since π-interaction is stronger at higher Ni coordination, on the Ni(100), the high coordination hollow-site becomes thermodynamically favored. Similar to the (100), at the Ni(110), the π-interaction at higher coordination is more favored, leading to the bridge-site preference. At the (110), the long-bridge and hollow adsorption sites cannot be considered as higher coordination sites as the M-C bond lengths are markedly larger leading to a significantly small overlap between orbitals and consequently, low adsorption energies. In the case of Ni(111), the same trend of higher-coordination sites preferences is expected, leading to the hollow-sites adsorption preferences. Based on the full repulsive nature of σ interaction in Ni, the hollow (hcp) adsorption site, where there is another Ni atom in the second surface layer beneath the CO, is more preferred than the hollow (fcc).

5.8 C-O bond-length Relation to Depth, Charge, and Metal-C bond-length

To understand the final geometrical structure of the CO molecule, we need to consider the factors that are affecting the CO structure and that determines the value of the final C-O bond length. Here, we consider the charge transferred from the metal to the CO molecule (***Q***), the depth of adsorption (***D***), and the metal-CO ($\boldsymbol{L_{m\text{-}c}}$) bond distance as the three main factors that are responsible for the C-O bond stretching. By adding those three factors into an equation that defines the final C-O bend-length, we can validate the relation between those three factors and the final C-O length (***L***). The equation is defined as follows:

$$\boxed{L = L_o + \frac{QDn}{L_{m-c}}} \qquad (5.1)$$

Where $\boldsymbol{L_o}$ is the initial C-O bond-length of the free CO molecule, and ***n*** is the empirical numerical factor with a value of 0.27 for both Ni and Cu.

The results in *Figure 32* show a matching behavior of the C-O bond length at different adsorption sites, in terms of variation with coordination number and amplitude. Only for the (110) surface, the amplitude of the C-O bonds is observed larger by ~ 0.03 Å. This amplitude shift can be attributed to the metal-CO bond distances that are generally larger than other surfaces, where other factors such as the dispersive van der Waal's forces should be considered in the equation. Adding dispersion corrections is found to bring the adsorption energetics closer to experimental values is the consideration of dispersive, van der Waals forces[14–16]. Nonetheless, adding dispersion corrections still leads to an

overestimated prediction of adsorption energies[16], which brings us back to the original problem with DFT inaccurate electronic structure predictions.

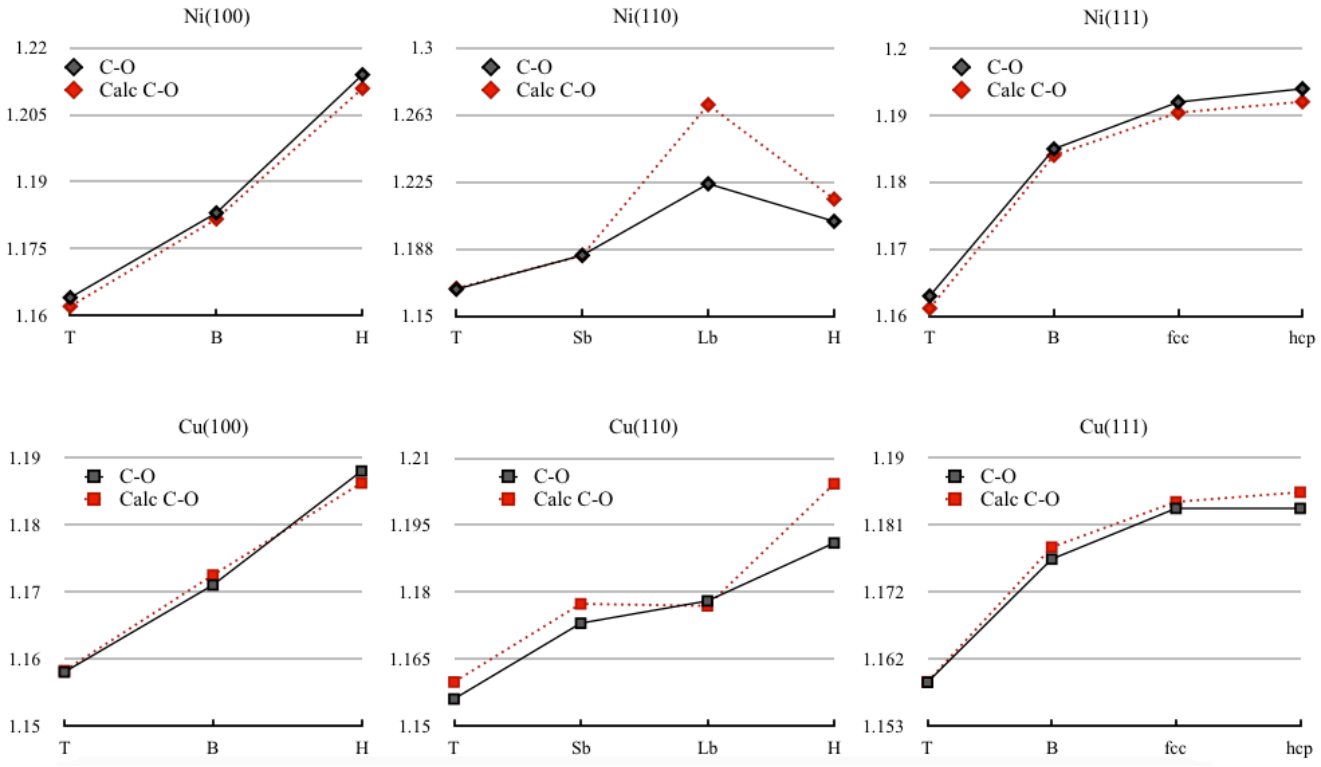

References

1. Blyholder, G. Molecular Orbital View of Chemisorbed Carbon Monoxide. *J. Phys. Chem.* (1964). doi:10.1021/j100792a006
2. Föhlisch, A. *et al.* The bonding of CO to metal surfaces. *J. Chem. Phys.* **112,** 1946–1958 (2000).
3. Stroppa, a, Termentzidis, K., Paier, J., Kresse, G. & Hafner, J. CO adsorption on metal surfaces: a hybrid functional study with plane wave basis set. *Phys. Rev. B* **76,** 32 (2007).
4. Scuseria, G. E., Miller, M. D., Jensen, F. & Geertsen, J. The dipole moment of carbon monoxide. *J. Chem. Phys.* **94,** 6660–6663 (1991).
5. Nilsson, A. & Pettersson, L. G. M. Chemical bonding on surfaces probed by X-ray emission spectroscopy and density functional theory. *Surface Science Reports* **55,** 49–167 (2004).
6. Gajdoš, M. & Hafner, J. CO adsorption on Cu(1 1 1) and Cu(0 0 1) surfaces: Improving site preference in DFT calculations. *Surf. Sci.* **590,** 117–126 (2005).
7. Vollmer, S., Witte, G. & Wöll, C. Determination of site specific adsorption energies of CO on copper. *Catal. Letters* **77,** 97–101 (2001).
8. Tracy, J. C. Structural influences on adsorption energy. III. CO on Cu(100). *J. Chem. Phys.* **56,** 2755–2761 (1972).
9. Andersson, S. & Pendry, J. Structure of co adsorbed on CU (100) and NI (100). *Phys. Rev. Lett.* (1979).
10. McConville, C. F. *et al.* An X-ray absorption and photoelectron diffraction study

of the Cu {100} c (2× 2) CO structure. *Surf. Sci.* **166,** 221–233 (1986).

11. Hofmann, P. *et al.* A photoelectron diffraction study of the structure of the Cu(110) (2×1)-CO system. *Surf. Sci.* **337,** 169–176 (1995).
12. Kessler, J. & Thieme, F. Chemisorption oF CO on Differently Prepared Cu(111) Surfaces. *Surf. Sci.* **67,** 405–415 (2000).
13. Kirstein, W., Krueger, B. & Thieme, F. CO adsorption studies on pure and Ni-covered Cu (111) surfaces. *Surf. Sci.* **176,** 505–529 (1986).
14. Moler, E. J. *et al.* Spatial structure determination of (√3×√3)R30° and (1.5×1.5)R18° CO or Cu(111) using angle-resolved photoemission extended fine structure. *Phys. Rev. B - Condens. Matter Mater. Phys.* **54,** 10862–10868 (1996).

Chapter 6

Conclusions and Future Work

We can conclude that studying CO adsorption mechanisms and charge transport phenomena using DFT calculations is a rather reliable method, and the contradicting energetics predictions do not necessarily imply inaccurate description of the surface chemical phenomena. This conclusion is based on the evidenced absence of correlation between adsorbate behavior or charge transport with the calculated adsorption energies. Based on the generalized gradient RPBE calculations, structural, energetics, and charge transfer properties are investigated for all available adsorption sites over distinctive Cu surface facets; (100), (110), and (111).

The study of the effect of varying surface facets on the adsorption process is demonstrated to be essential for a profound understanding of the adsorbed molecule behavior and final geometrical shape. The effect of surface atomic arrangement at different facets helped in getting insights on the reason behind the contradicting DFT site-preference predictions. It has been confirmed that the energy positioning of the frontier (5σ and $2\pi^*$) orbitals relative to the metallic *d*- band center is the determining factor for adsorption site preference. However, it is additionally claimed that the surface bonding magnitude is also affected by the density of overlapping metallic orbitals with the right symmetry to interact with the CO frontier orbitals. The interplay between the spatial and energy distance between interacting orbitals is a successful tool in explaining the on-top site preference prediction for the Cu(100) and the short-bridge and hollow site preferences predicted for the Cu(110) and Cu(111), respectively. The consideration of factors, such as the effect of

the distinctive atomic arrangements at different facets, must therefore be considered for a better analysis of the stubborn CO adsorption puzzle. Finally, the importance of considering orbitals other than the frontier orbitals, such as the 3σ and 1π orbitals, is verified to be essential for understanding the discrepancies between the adsorbate behavior at the same adsorption site at different facets. The behavior of the CO molecule is thus compared at each site in terms of the 3σ and 1π orbitals, which hold the internal C-O bonding. Since the 3σ and 1π orbitals holds the internal C-O triple bond, the different orbital behaviors at each site resulted in a different geometrical structure of the CO molecule. It is confirmed that the energy upshift of the orbitals reflects a destabilization of the internal bonding. In addition, the broadening of the 1π peak, which implies a splitting of the 1π orbitals, also reflected a C-O internal bond destabilization, however, the effect of the orbital splitting on the internal bond stability is found to be more effectual than the energy upshifts.

In addition, the parameters that determine the final structural properties of the adsorbed CO molecule are validated with an empirical equation, where the increase of the adsorption depth and charge transfer from the metal orbitals to the CO molecule have proved a direct influence on the CO destabilization, whereas the increase of metal-carbon bond length had an inverse effect and lead to the stabilization of the CO molecule.

In the future, we are aiming to expand this investigation to encompass a wider range of substrate materials, specifically transition metals with different occupancies of the d-orbital. A further goal that we have is to deeply investigate the true nature of σ-bonding, which remains a controversy in literature till this date. In this work, we presented a

plausible assumption of a dual nature of the σ-interaction, with both attractive and repulsive characters that vary according to the type of substrate and adsorption site. This assumption is supported with our charge population data. However, to emphasize the true nature of σ-bonding, further calculations of sub-orbitals energy perturbations are needed to be carried out meticulously.

We hope that the presented new insights on the effect of surface atoms arrangement and the consideration of the full orbitals perturbations of the adsorbate molecule will open the doors for a more profound understanding of the surface chemical bonding

PUBLICATIONS

1. Kareem M. Gameel, Icell M. Sharafaldin, Amr U. Abourayya, Ahmed H. Biby, Nageh K. Allam, "*Unveiling CO Adsorption on Cu Surfaces: New Insights from Molecular Orbital Principles*", PCCP Journal (Manuscript under review)
2. Kareem M. Gameel*, Sarah A. Tolba*, Basant A. Ali, Hossam A. Almossalami, Nageh K. Allam, "*The DFT+U: Approaches, Accuracy, and Applications",* Book Chapter in the *"DFT Calculations: Recent Progresses of Theory and Application*" Intech Book , Edited by Gang Yang, May 2018.